

1 **Trends in atmospheric evaporative demand in Great Britain**  
2 **using high-resolution meteorological data**

3

4 **Emma L. Robinson<sup>1</sup>, Eleanor M. Blyth<sup>1</sup>, Douglas B. Clark<sup>1</sup>, Jon Finch<sup>1</sup> and Alison**  
5 **C. Rudd<sup>1</sup>**

6 [1]{Centre for Ecology and Hydrology, Maclean Building, Benson Lane, Crowmarsh Gifford,  
7 Wallingford OX10 8BB }

8 Correspondence to: Emma L. Robinson (emrobi@ceh.ac.uk)

9

## 10 **Abstract**

11 Observations of climate are often available on very different spatial scales from observations  
12 of the natural environments and resources that are affected by climate change. In order to help  
13 bridge the gap between these scales using modelling, a new dataset of daily meteorological  
14 variables was created at 1 km resolution over Great Britain for the years 1961-2012, by  
15 interpolating coarser resolution climate data and including the effects of local topography.  
16 These variables were used to calculate atmospheric evaporative demand (AED) at the same  
17 spatial and temporal resolution. Two functions that represent AED were chosen: one is a  
18 standard form of Potential Evapotranspiration (PET) and the other is a derived PET measure  
19 used by hydrologists that includes the effect of water intercepted by the canopy (PETI).  
20 Temporal trends in these functions were calculated, with PET found to be increasing in all  
21 regions, and at an overall rate of  $0.021 \pm 0.021 \text{ mm d}^{-1} \text{ decade}^{-1}$  in Great Britain. PETI was found  
22 to be increasing at a rate of  $0.019 \pm 0.020 \text{ mm d}^{-1} \text{ decade}^{-1}$  in Great Britain, but this was not  
23 statistically significant. However, there was a trend in PETI in England of  $0.023 \pm 0.023 \text{ mm d}^{-1} \text{ decade}^{-1}$ .  
24 The trends were found to vary by season, with spring PET increasing by  $0.043 \pm 0.019$   
25  $\text{mm d}^{-1} \text{ decade}^{-1}$  ( $0.038 \pm 0.018 \text{ mm d}^{-1} \text{ decade}^{-1}$  when the interception correction is included) in  
26 Great Britain, while there is no statistically significant trend in other seasons. The trends were  
27 attributed analytically to trends in the climate variables; the overall positive trend was  
28 predominantly driven by rising air temperature, although rising specific humidity had a negative  
29 effect on the trend. Recasting the analysis in terms of relative humidity revealed that the overall  
30 effect is that falling relative humidity causes the PET to rise. Increasing downward short- and  
31 longwave radiation made an overall positive contribution to the PET trend, while decreasing  
32 wind speed made a negative contribution to the trend in PET. The trend in spring PET was  
33 particularly strong due to a strong decrease in relative humidity and increase in downward  
34 shortwave radiation in the spring.

35

## 36 **1 Introduction**

37 There are many studies showing the ways in which our living environment is changing over  
38 time: changing global temperatures (IPCC, 2013), radiation (Wild, 2009) and wind speeds  
39 (McVicar et al., 2012) can have significant impacts on ecosystems and human life (IPCC,  
40 2014a). While there are overall global trends, the impacts can vary between regions (IPCC,  
41 2014b). In the UK, wildlife surveys of both flora (Wood et al., 2015; Evans et al., 2008) and  
42 fauna (Pocock et al., 2015) show a shift in patterns and timing (Thackeray et al., 2010). In  
43 addition, the UK natural resources of freshwater (Watts et al., 2015), soils (Reynolds et al.,  
44 2013; Bellamy et al., 2005) and vegetation (Berry et al., 2002; Hickling et al., 2006; Norton et  
45 al., 2012) are changing. The UK is experiencing new environmental stresses on the land and  
46 water systems through changes in temperature and river flows (Crooks and Kay, 2015; Watts  
47 et al., 2015; Hannaford, 2015), which are part of a widespread global pattern of temperature  
48 increase and circulation changes (Watts et al., 2015).

49 To explain these changes in terms of climate drivers, there are several gridded meteorological  
50 datasets available at global and regional scales. Global datasets can be based on observations –  
51 for example the 0.5° resolution Climate Research Unit time series 3.21 (CRU TS 3.21) data  
52 (Jones and Harris, 2013; Harris et al., 2014) – while some are based on global meteorological  
53 reanalyses bias-corrected to observations – for example the WATCH Forcing Data (WFD, 0.5°;  
54 Weedon et al. (2011)), the WATCH Forcing Data methodology applied to ERA-Interim  
55 reanalysis product (WFDEI, 0.5°; Weedon et al. (2014)) and the Princeton Global  
56 Meteorological Forcing Dataset (0.25°–1°; Sheffield et al. (2006)). At the regional scale in  
57 Great Britain (GB), there are datasets that are derived directly from observations – for example  
58 the Met Office Rainfall and Evaporation Calculation System (MORECS) dataset at 40 km  
59 resolution (Thompson et al., 1981; Hough and Jones, 1997; Field, 1983) and the UKCP09  
60 observed climate data at 5 km resolution (Jenkins et al., 2008).

61 However, while regional observations of carbon, methane and water emissions from the land  
62 (Baldocchi et al., 1996), the vegetation cover (Morton et al., 2011) and soil properties  
63 (FAO/IIASA/ISRIC/ISS-CAS/JRC, 2012) are typically made at the finer landscape scale of  
64 100 m to 1000 m, most of these long-term gridded meteorological datasets are only available  
65 at a relatively coarse resolution of a few tens of km. These spatial scales may not be  
66 representative of the climate experienced by the flora and fauna being studied, and it has also  
67 been shown that input resolution can have a strong effect on the performance of hydrological

68 models (Kay et al., 2015). In addition, the coarse temporal resolution of some datasets, for  
69 example the monthly CRU TS 3.21 data (Harris et al., 2014; Jones and Harris, 2013), can miss  
70 important sub-monthly extremes.

71 Regional studies are important to identify drivers and impacts of changing meteorology that  
72 may or may not be reflected in trends in global means. For example, in Canada (Vincent et al.,  
73 2015) and Europe (Fleig et al., 2015), high resolution meteorological data have been used to  
74 identify the impacts of changing circulation patterns, while in Australia wind speed data have  
75 been used to quantify the effects of global stilling in the region (McVicar et al., 2008). While  
76 there are datasets available at finer spatial and temporal resolutions for the UK (such as  
77 UKCP09 (Jenkins et al., 2008)), these often do not provide all the variables needed to identify  
78 the impacts of changing climate.

79 To address this, we have created a meteorological dataset for Great Britain at 1 km resolution:  
80 the Climate Hydrology and Ecology research Support System meteorology dataset for Great  
81 Britain (1961-2012) (CHESS-met; Robinson et al. (2015b)). It is derived from the observation-  
82 based MORECS dataset (Thompson et al., 1981; Hough and Jones, 1997), and then downscaled  
83 using information about topography. This is augmented by an independent precipitation dataset  
84 – Gridded Estimates of daily and monthly Areal Rainfall for the United Kingdom (CEH-GEAR;  
85 Tanguy et al. (2014); Keller et al. (2015)) – along with variables from two global datasets –  
86 WFD and CRU TS 3.21 – to produce a comprehensive, observation-based, daily meteorological  
87 dataset at 1 km × 1 km spatial resolution.

88 In order to understand the effect of meteorology on the water cycle, a key variable in  
89 hydrological modelling is the atmospheric evaporative demand (AED), which is determined by  
90 meteorological variables (Kay et al., 2013). It has been shown that water-resource and  
91 hydrological model results are largely driven by how this property is defined and used  
92 (Haddeland et al., 2011). The AED can be expressed in several ways, for instance the  
93 evaporation from a wet surface, from a well-watered but dry uniform vegetated cover, or from  
94 a hypothetical well-watered but dry version of the actual vegetation. Metrics such as the Palmer  
95 Drought Severity Index (PDSI; Palmer (1965)) use potential evapotranspiration (PET) as an  
96 input to represent AED, while many hydrological models such as Climate and Land use  
97 Scenario Simulation in Catchments (CLASSIC; Crooks and Naden (2007)) or Grid-to-Grid  
98 (G2G; Bell et al. (2009)), which also require an input representing AED, use a distinct form of  
99 the PET which includes the intercepted water from rainfall (this is described later in the text)

100 which we hereby name PETI. While hydrological models can make use of high resolution  
101 topographic information and precipitation datasets, they are often driven with PET calculated  
102 at a coarser resolution (Bell et al., 2011; Bell et al., 2012; Kay et al., 2015). Therefore, we have  
103 also created a 1 km × 1 km resolution dataset, the Climate Hydrology and Ecology research  
104 Support System Potential Evapotranspiration dataset for Great Britain (1961-2012) (CHESS-  
105 PE; Robinson et al. (2015a)), consisting of estimates of PET and PETI, which can be used to  
106 run high-resolution hydrological models.

107 Other regional studies have created gridded estimates of AED in Austria (Haslinger and  
108 Bartsch, 2016) and Australia (Donohue et al., 2010). Regional studies of trends in AED have  
109 seen varied results, with increasing AED seen in Romania (Paltineanu et al., 2012), Serbia  
110 (Gocic and Trajkovic, 2013), Spain (Vicente-Serrano et al., 2014), some regions of China (Li  
111 and Zhou, 2014) and Iran (Azizzadeh and Javan, 2015; Hosseinzadeh Talaei et al., 2013; Tabari  
112 et al., 2012), decreasing AED in north east India (Jhajharia et al., 2012) and regions in China  
113 (Yin et al., 2009; Song, 2010; Shan et al., 2015; Zhao et al., 2015; Zhang et al., 2015; Lu et al.,  
114 2016) and regional variability in Australia (Donohue et al., 2010) and China (Li et al., 2015).  
115 In order to understand this variability, it is important to quantify the relative contributions of  
116 the changing meteorological variables to trends in AED and regional studies often find different  
117 drivers of changing AED (see McVicar et al. (2012) for a review). Relative humidity has been  
118 shown to drive AED in the Canary Islands (Vicente-Serrano et al., 2016), wind speed and air  
119 temperature were shown to have nearly equal but opposite effects in Australia (Donohue et al.,  
120 2010), while in China sunshine hours (Li et al., 2015), wind speed (Yin et al., 2009) or a  
121 combination of the two (Lu et al., 2016) have been shown to drive trends. Rudd and Kay (2015)  
122 investigated projected changes in PET using a regional climate model, but little has been done  
123 to investigate historical trends of AED in the UK.

124 The objectives of this paper are (i) to evaluate the trends in key meteorological variables in  
125 Great Britain over the years 1961-2012; (ii) to evaluate the AED in Great Britain over the same  
126 time period using PET; (iii) to investigate the effect of including interception in the formulation  
127 of PET called PETI; (iv) to evaluate trends in PET over the time period of interest; and (v) to  
128 attribute the trends in PET to trends in meteorological variables. To address these objectives,  
129 the paper is structured as follows. Section 2 presents the calculation of the meteorological  
130 variables. Section 3 presents the calculation of PET and PETI from the meteorological variables  
131 and assesses the difference between PET and PETI. In Section 4 the trends of the meteorological

132 variables and AED are calculated and the trends in PET are attributed to trends in  
133 meteorological variables. In Section 5 the results are discussed and conclusions are presented  
134 in Section 6.

## 135 **2 Calculation of meteorological variables**

136 The meteorological variables included in this new dataset (Robinson et al., 2015b) are daily  
137 mean values of air temperature, specific humidity, wind speed, downward longwave (LW) and  
138 shortwave (SW) radiation, precipitation and air pressure, plus daily temperature range (Table  
139 1). These variables are important drivers of near-surface conditions, and, for instance, are the  
140 full set of variables required to drive the JULES land surface model (LSM) (Best et al., 2011;  
141 Clark et al., 2011), as well as other LSMs.

142 The data were derived primarily from MORECS, which is a long-term gridded dataset starting  
143 in 1961 and updated to the present (Thompson et al., 1981; Hough and Jones, 1997). It  
144 interpolates five variables from synoptic stations (daily mean values of air temperature, vapour  
145 pressure and wind speed, daily hours of bright sunshine and daily total precipitation) to a 40  
146 km × 40 km resolution grid aligned with the Ordnance Survey National Grid. There are  
147 currently 270 stations reporting in real time, while a further 170 report the daily readings on a  
148 monthly basis, but numbers have varied throughout the run. The algorithm interpolates a  
149 varying number of stations (up to nine) for each square, depending on data availability (Hough  
150 and Jones, 1997). The interpolation is such that the value in each grid square is the effective  
151 measurement of a station positioned at the centre of the square and at the grid square mean  
152 elevation, averaged from 00:00 GMT to 00:00 GMT the next day. MORECS is a consistent,  
153 quality-controlled time series, which accounts for changing station coverage. The MORECS  
154 variables were used to derive the air temperature, specific humidity, wind speed, downward  
155 LW and SW radiation and air pressure in the new dataset. The WFD and CRU TS 3.21 datasets  
156 were used for surface air pressure and daily temperature range respectively, as they could not  
157 be calculated solely from MORECS. Additionally precipitation was obtained from the CEH-  
158 GEAR data, which is a product directly interpolated to 1 km from the station data (Keller et al.,  
159 2015).

160 The spatial coverage of the dataset was determined by the spatial coverage of MORECS, which  
161 covers the majority of Great Britain, but excludes some coastal regions and islands at the 1 km  
162 scale. For most of these points, the interpolation was extended from the nearest MORECS

163 squares, but some outlying islands (in particular Shetland and the Scilly Isles) were excluded  
164 when the entire island was further than 40 km from the nearest MORECS square.

## 165 **2.1 Air temperature**

166 Air temperature,  $T_a$  (K), was derived from the MORECS air temperature. The MORECS air  
167 temperature was reduced to mean sea level, using a lapse rate of  $-0.006 \text{ K m}^{-1}$  (Hough and  
168 Jones, 1997). A bicubic spline was used to interpolate from 40 km resolution to 1 km resolution,  
169 then the temperatures were adjusted to the elevation of each 1 km square using the same lapse  
170 rate. The 1 km resolution elevation data used were aggregated from the Integrated Hydrological  
171 Digital Terrain Model (IHDTM) – a 50 m resolution digital terrain model (Morris and Flavin,  
172 1990).

## 173 **2.2 Specific humidity**

174 Specific humidity,  $q_a$  ( $\text{kg kg}^{-1}$ ), was derived from the MORECS vapour pressure,  $e_M$  (Pa), which  
175 was first reduced to mean sea level, using the equation

$$176 \quad e_{sea} = e_M \left( 1 - \frac{L_e}{100} h_M \right) \quad (1)$$

177 where  $L_e$  is the lapse rate of  $-0.025 \text{ \% m}^{-1}$  and  $h$  is the elevation of the MORECS square  
178 (Thompson et al., 1981). The actual lapse rate of humidity will, in general, vary according to  
179 atmospheric conditions. However, calculating this would require more detailed information  
180 than is available in the input data used. Any method of calculating the variation of specific  
181 humidity with height will involve several assumptions, but the method used here is well-  
182 established and is used by the Met Office in calculating MORECS (Thompson et al., 1981).  
183 The value of the vapour pressure lapse rate is chosen to keep relative humidity approximately  
184 constant with altitude, rather than assuming that the vapour pressure itself is constant.

185 A bicubic spline was used to interpolate vapour pressure to 1 km resolution then the values  
186 were adjusted to the 1 km resolution elevation using the IHDTM elevations and using the same  
187 lapse rate, such that

$$188 \quad e = e_{sea,1km} \left( 1 + \frac{L_e}{100} h_{1km} \right), \quad (2)$$

189 where  $e_{sea,1km}$  is the sea-level vapour pressure at 1 km resolution and  $h_{1km}$  is the 1 km resolution  
190 elevation.

191 Finally the specific humidity was calculated, using

$$192 \quad q_a = \frac{\epsilon e}{p_*(1-\epsilon)e}, \quad (3)$$

193 where  $e$  is the vapour pressure (Pa) and  $\epsilon = 0.622$  is the mass ratio of water to dry air (Gill,  
194 1982). The air pressure,  $p_*$ , in this calculation was assumed to have a constant value of 100000  
195 Pa because this was prescribed in the computer code. It would be better to use a varying air  
196 pressure, as calculated in Section 2.8, but this makes a negligible difference (of a few percent)  
197 to the calculated specific humidity, and to the PET and PETI calculated in Section 3, and a  
198 constant  $p_*$  was retained.

### 199 **2.3 Downward shortwave radiation**

200 Downward SW radiation,  $S_d$  ( $\text{W m}^{-2}$ ), was derived from the MORECS hours of bright sunshine  
201 (defined as the total number of hours in a day for which solar irradiation exceeds  $120 \text{ W m}^{-2}$   
202 (WMO, 2013)). The value calculated is the mean SW radiation over 24 hours. The sunshine  
203 hours were used to calculate the cloud cover factor,  $C_f = n/N$ , where  $n$  is the number of hours  
204 of bright sunshine in a day, and  $N$  is the total number of hours between sunrise and sunset  
205 (Marthews et al., 2011). The cloud cover factor was interpolated to 1 km resolution using a  
206 bicubic spline. The downward SW solar radiation for a horizontal plane at the Earth's surface  
207 was then calculated using the solar angle equations of Iqbal (1983) and a form of the Ångström-  
208 Prescott equation which relates hours of bright sunshine to solar irradiance (Ångström, 1918;  
209 Prescott, 1940), with empirical coefficients calculated by Cowley (1978). They vary spatially  
210 and seasonally and effectively account for reduction of irradiance with increasing solar zenith  
211 angle, as well as implicitly accounting for spatially- and seasonally-varying aerosol effects.  
212 However, they do not vary interannually and thus do not explicitly include long-term trends in  
213 aerosol concentration.

214 The downward SW radiation was then corrected for the average inclination and aspect of the  
215 surface, assuming that only the direct beam radiation is a function of the inclination and that  
216 the diffuse radiation is homogeneous. It was also assumed that the cloud cover is the dominant  
217 factor in determining the diffuse fraction (Muneer and Munawwar, 2006). The aspect and  
218 inclination were calculated using the IHDTM elevation at 50 m resolution, following the  
219 method of Horn (1981), and were then aggregated to 1 km resolution. The top of atmosphere  
220 flux for horizontal and inclined surfaces was calculated following Allen et al. (2006) and the  
221 ratio used to scale the direct beam radiation.



## 222 **2.4 Downward longwave radiation**

223 Downward LW radiation,  $L_d$  ( $\text{W m}^{-2}$ ), was derived from the 1 km resolution air temperature  
224 (Sect. 2.1), vapour pressure (Sect. 2.2) and cloud cover factor (Sect. 2.3). The downward LW  
225 radiation for clear sky conditions was calculated as a function of air temperature and  
226 precipitable water using the method of Dilley and O'Brien (1998), with precipitable water  
227 calculated from air temperature and humidity following Prata (1996). The additional  
228 component due to cloud cover was calculated using the equations of Kimball et al. (1982),  
229 assuming a constant cloud base height of 1000 m.

## 230 **2.5 Wind speed**

231 The wind speed at a height of 10 m,  $u_{10}$  ( $\text{m s}^{-1}$ ), was derived from the MORECS 10 m wind  
232 speed, which were interpolated to 1 km resolution using a bicubic spline and adjusted for  
233 topography using a 1 km resolution dataset of mean wind speeds produced by the UK Energy  
234 Technology Support Unit (ETSU; Newton and Burch (1985); Burch and Ravenscroft (1992)).  
235 This used Numerical Objective Analysis Boundary Layer (NOABL) methodology combined  
236 with station wind measurements over the period 1975-84 to produce a map of mean wind speed  
237 over the UK. To calculate the topographic correction, the ETSU wind speed was aggregated to  
238 40 km resolution, then the difference between each 1 km value and the corresponding 40 km  
239 mean found. This difference was added to the interpolated daily wind speed. In cases where  
240 this would result in a negative wind speed, the wind speed was set to zero.

## 241 **2.6 Precipitation**

242 Precipitation rate,  $P$  ( $\text{kg m}^{-2} \text{s}^{-1}$ ), is taken from the daily CEH-GEAR dataset (Tanguy et al.,  
243 2014; Keller et al., 2015), scaled to the appropriate units. The CEH-GEAR methodology uses  
244 natural neighbour interpolation (Gold, 1989) to interpolate synoptic station data to a 1 km  
245 resolution gridded daily dataset of the estimated precipitation in 24 hours between 09:00 GMT  
246 and 09:00 GMT the next day.

## 247 **2.7 Daily temperature range**

248 Daily temperature range (DTR),  $D_T$  (K), was obtained from the CRU TS 3.21 monthly mean  
249 daily temperature range estimates on a  $0.5^\circ$  latitude  $\times$   $0.5^\circ$  longitude grid, which is interpolated  
250 from monthly climate observations (Harris et al., 2014; Jones and Harris, 2013). There is no

251 standard way to correct DTR for elevation, so these data were reprojected to the 1 km grid with  
252 no interpolation and the monthly mean used to populate the daily values in each month.  
253 Although DTR is not required in the calculation of AED, it is a required input of the JULES  
254 LSM, in order to run at sub-daily timestep with daily input data.

## 255 **2.8 Surface air pressure**

256 Surface air pressure,  $p^*$  (Pa), was derived from the WFD, an observation-corrected reanalysis  
257 product, which provides 3 hourly meteorological data for 1958-2001 on a  $0.5^\circ$  latitude  $\times$   $0.5^\circ$   
258 longitude resolution grid (Weedon et al., 2011). Mean monthly values of WFD surface air  
259 pressure and air temperature were calculated for each  $0.5^\circ$  grid box over the years 1961-2001.  
260 These were reprojected to the 1 km grid with no interpolation, then the lapse rate of air  
261 temperature (Sect. 2.1) used to calculate the integral of the hypsometric equation (Shuttleworth,  
262 2012), in order to obtain the air pressure at the elevation of each 1 km grid. The mean monthly  
263 values were used to populate the daily values in the full dataset, thus the surface air pressure in  
264 the new dataset does not vary interannually, but does vary seasonally. This is reasonable as the  
265 trend in surface air pressure in the WFD is negligible (Weedon et al., 2011).

## 266 **2.9 Spatial and seasonal patterns of meteorological variables**

267 Long-term mean values of the meteorological variables were calculated for each 1 km square  
268 over the whole dataset, covering the years 1961-2012 (Fig. 1). Four sub-regions of interest were  
269 defined (Fig. 2); three of these regions correspond to nations (England, Wales and Scotland),  
270 while the fourth is the ‘English lowlands’, a subset of England, covering south-central and  
271 south-east England, East Anglia and the East Midlands (Folland et al., 2015). Mean-monthly  
272 climatologies were calculated over the whole of Great Britain (GB), and over these four regions  
273 of interest (Fig. 3).

274 The maps clearly show the effect of topography on the variables (Fig. 1), with an inverse  
275 correlation between elevation and temperature, specific humidity, downward LW radiation and  
276 surface air pressure and a positive correlation with wind speed. The precipitation has an east-  
277 west gradient due to prevailing weather systems and orography. The fine-scale structure of the  
278 downward SW radiation is due to the aspect and elevation of each grid cell, with more spatial  
279 variability in areas with more varying terrain. As no topographic correction has been applied to  
280 DTR, it varies only on a larger spatial scale. Although specific humidity is inversely

281 proportional to elevation, relative humidity is not, as the saturated specific humidity will also  
282 be inversely proportional to elevation due to the decrease in temperature with height. The strong  
283 correlation between wind speed and elevation means that it is very variable over short spatial  
284 scales, particularly in Scotland.

285 The mean-monthly climatologies (Fig. 3) demonstrate the differences between the regions, with  
286 Scotland generally having lower temperatures and more precipitation than the average, and  
287 England (particularly the English lowlands) being warmer and drier.

## 288 **2.10 Validation of meteorology**

289 The precipitation dataset, CEH-GEAR, has previously been validated against observations  
290 (Keller et al., 2015). Other studies discuss the uncertainties in the CRU TS 3.21 daily  
291 temperature range data (Harris et al., 2014) and WFDEI air pressure data (Weedon et al., 2014).

292 For the other variables, the MORECS data set is ultimately derived from the synoptic stations  
293 around the UK which represent most of the available observed meteorological data for the  
294 country. The only way to validate the gridded meteorology presented here is to compare it to  
295 independently observed data, which are available at a few sites where meteorological  
296 measurement stations that are not part of the synoptic network are located. Here we carry out a  
297 validation exercise with data from four sites from the UK, which have meteorological  
298 measurements available for between 5 and 10 years. Details of the sites and data are in  
299 Appendix A. Fig. 4 shows the comparison of data set air temperature with the observed air  
300 temperature at each of the four sites. This shows a strong correlation ( $r^2$  between 0.94 and 0.97)  
301 between the data set and the observations. Fig. 5 shows the mean-monthly climatology  
302 calculated from both the data set and from the observations (only for times for which  
303 observations were available) and demonstrates that the data set successfully captures the  
304 seasonal cycle. This has been repeated for downward SW radiation and for an estimate of the  
305 mixing ratio of water vapour, 10 m wind speed and surface air pressure (Appendix A). The air  
306 temperature, downward SW radiation and mixing ratio all have high correlations and represent  
307 the seasonal cycle well. The downward SW is overestimated at Auchencorth Moss, which may  
308 be due to local factors (e.g. shading, or the siting of the station within the grid square). The  
309 wind speed is overestimated by the derived data set at two sites, which is likely to be due to  
310 land cover effects. The modelling which produced the ETSU dataset uses topography but not  
311 land cover (Burch and Ravenscroft, 1992; Newton and Burch, 1985), so at sites with tall

312 vegetation the wind speed is likely to be less than the modelled value. The air pressure has a  
 313 low correlation because the data set contains a mean-monthly climatological value. However,  
 314 the mean bias is low and the RMSE is small, confirming that it is reasonable to use a  
 315 climatological value in place of daily data.

### 316 **3 Calculation of potential evapotranspiration (PET)**

317 There are several ways to assess the evaporative demand of the atmosphere. Pan evaporation  
 318 can be modelled using the Pen-Pan model (Rotstayn et al., 2006), or open-water evaporation  
 319 can be modelled with the Penman equation (Penman, 1948). However, neither of these account  
 320 for the fact that in general the evaporation is occurring from a vegetated surface. A widely used  
 321 model is the Penman-Monteith PET,  $E_p$  ( $\text{mm d}^{-1}$ , equivalent to  $\text{kg m}^{-2} \text{d}^{-1}$ ), which is a physically-  
 322 based formulation of AED (Monteith, 1965), including the effect of stomatal resistance. It  
 323 provides an estimate of AED dependent on the atmospheric conditions but allowing for the fact  
 324 that the water is evaporating through the surface of leaves and thus the resistance is higher. It  
 325 can be calculated from the daily meteorological variables using the equation

$$326 \quad E_p = \frac{t_d}{\lambda} \frac{\Delta A + \frac{c_p \rho_a}{r_a} (q_s - q_a)}{\Delta + \gamma \left(1 + \frac{r_s}{r_a}\right)}, \quad (4)$$

327 where  $t_d = 86400 \text{ s d}^{-1}$  is the length of a day,  $\lambda = 2.5 \times 10^6 \text{ J kg}^{-1}$  is the latent heat of evaporation,  
 328  $q_s$  is saturated specific humidity ( $\text{kg kg}^{-1}$ ),  $\Delta$  is the gradient of saturated specific humidity with  
 329 respect to temperature ( $\text{kg kg}^{-1} \text{K}^{-1}$ ),  $A$  is the available energy ( $\text{W m}^{-2}$ ),  $c_p = 1010 \text{ J kg}^{-1} \text{K}^{-1}$  is the  
 330 specific heat capacity of air,  $\rho_a$  is the density of air ( $\text{kg m}^{-3}$ ),  $q_a$  is specific humidity ( $\text{kg kg}^{-1}$ ),  
 331  $\gamma = 0.004 \text{ K}^{-1}$  is the psychrometric constant,  $r_s$  is stomatal resistance ( $\text{s m}^{-1}$ ) and  $r_a$  is aerodynamic  
 332 resistance ( $\text{s m}^{-1}$ ) (Stewart, 1989).

333 The saturated specific humidity,  $q_s$  ( $\text{kg kg}^{-1}$ ), is calculated from saturated vapour pressure,  $e_s$   
 334 (Pa), using Eq. 3. The saturated vapour pressure is calculated using an empirical fit to air  
 335 temperature

$$336 \quad e_s = p_{sp} \exp\left(\sum_{i=1}^4 a_i \left(1 - \frac{T_{sp}}{T_a}\right)^i\right), \quad (5)$$

337 where  $p_{sp} = 101325 \text{ Pa}$  is the steam point pressure,  $T_{sp} = 373.15 \text{ K}$  is the steam point temperature  
 338 and  $a = (13.3185, -1.9760, -0.6445, -0.1299)$  are empirical coefficients (Richards, 1971).

339 The derivative of the saturated specific humidity with respect to temperature,  $\Delta$  ( $\text{kg kg}^{-1} \text{K}^{-1}$ ),  
 340 is therefore

$$341 \quad \Delta = \frac{T_{sp}}{T_a^2} \frac{p_* q_s}{p_* - (1-\epsilon)e_s} \sum_{i=1}^4 i a_i \left(1 - \frac{T_{sp}}{T_a}\right)^{i-1}, \quad (6)$$

342 where the air pressure used is the spatially varying air pressure calculated in Sect.2.8.

343 The available energy,  $A$  ( $\text{W m}^{-2}$ ), is the energy balance of the surface,

$$344 \quad A = R_n - G, \quad (7)$$

345 where  $R_n$  is the net radiation ( $\text{W m}^{-2}$ ) and  $G$  is the soil heat flux ( $\text{W m}^{-2}$ ). The net soil heat flux  
346 is negligible at the daily timescale (Allen et al., 1998), so the available energy is equal to the  
347 net radiation, such that

$$348 \quad A = (1 - \alpha)S_d + \varepsilon(L_d - \sigma T_*^4), \quad (8)$$

349 where  $\sigma$  is the Stefan-Boltzmann constant,  $\alpha$  is the albedo and  $\varepsilon$  the emissivity of the surface  
350 and  $T_*$  is the surface temperature (Shuttleworth, 2012). For this study we make the simplifying  
351 assumption that the surface temperature is approximately equal to the air temperature,  $T_a$  and  
352 use the latter in Eq. 8.

353 The air density,  $\rho_a$  ( $\text{kg m}^{-3}$ ), is a function of air pressure and temperature,

$$354 \quad \rho_a = \frac{p_*}{r T_a}, \quad (9)$$

355 where  $r = 287.05 \text{ J kg}^{-1} \text{ K}^{-1}$  is the gas constant of air and the air pressure used is the spatially  
356 varying air pressure calculated in Sect. 2.8.

357 The stomatal and aerodynamic resistances are strongly dependent on land cover due to  
358 differences in roughness length and physiological constraints on transpiration of different  
359 vegetation types. In addition, the albedo and emissivity are also dependent on the land cover.  
360 In order to investigate the effect of meteorology on AED, as distinct from land use effects, the  
361 PET was calculated for a single land cover type over the whole of the domain. If necessary, this  
362 can be adjusted to give an estimate of PET specific to the local land cover, for example using  
363 regression relationships (Crooks and Naden, 2007). As a standard, the Food and Agriculture  
364 Organization of the United Nations (FAO) calculate reference crop evaporation for a  
365 hypothetical reference crop, which corresponds to a well-watered grass (Allen et al., 1998).  
366 Following this, the PET in the current study was calculated for a reference crop of 0.12 m  
367 height, with constant stomatal resistance,  $r_s = 70.0 \text{ s m}^{-1}$ , an albedo of 0.23 and emissivity of  
368 0.92 over the whole of Great Britain. This study therefore neglects the effect of land-use on

369 evaporation, which could be investigated in future by calculating PET for different land surface  
370 types, with different coverage for each year of the dataset.

371 In general, aerodynamic resistance is a function of wind speed and canopy height. Following  
372 Allen et al. (1998), the aerodynamic resistance,  $r_a$  ( $s\ m^{-1}$ ), of a reference crop of 0.12 m height  
373 is a function of the 10 m wind speed

$$374 \quad r_a = \frac{278}{u_{10}}. \quad (10)$$

375 Note that, since the wind speed is likely to be biased high at sites with tall vegetation (Sect.  
376 2.10), this implies that the aerodynamic resistance is likely to be biased low, leading to an  
377 overestimate of PET. However, the estimate of PET here is for a reference crop over the whole  
378 of the dataset, and does not consider the effect of tall vegetation, so the wind speed is  
379 appropriate.

380 Thus the PET is a function of six of the meteorological variables: air temperature, specific  
381 humidity, downward LW and SW radiation, wind speed and surface air pressure.

382 To explore the role of the different meteorological variables in the AED, it is helpful to split  
383 the radiative component (the first part of the numerator in Eq. 4) from the wind component (the  
384 second part). Formally, this is defined as follows (Doorenbos, 1977):

385 The radiative component,  $E_{PR}$ ,

$$386 \quad E_{PR} = \frac{t_d}{\lambda} \frac{\Delta A}{\Delta + \gamma \left(1 + \frac{r_s}{r_a}\right)}, \quad (11)$$

387 and the aerodynamic component,  $E_{PA}$ ,

$$388 \quad E_{PA} = \frac{t_d}{\lambda} \frac{c_p \rho_a (q_s - q_a)}{\Delta + \gamma \left(1 + \frac{r_s}{r_a}\right)}, \quad (12)$$

389 such that  $E_P = E_{PR} + E_{PA}$ .

### 390 **3.1 Potential evapotranspiration with interception (PETI)**

391 When rain falls, water is intercepted by the canopy. The evaporation of this water is not  
392 constrained by stomatal resistance but is subject to the same aerodynamic resistance as  
393 transpiration (Shuttleworth, 2012). At the same time, transpiration is inhibited in a wet canopy.  
394 Suppression of transpiration is well observed both by comparing eddy-covariance fluxes and  
395 observations of sap flow (Kume et al., 2006; Moors, 2012), and by observing stomatal and

396 photosynthesis response to wetting (Ishibashi and Terashima, 1995). For plants which have at  
397 least some of their stomata on the upper surface of the leaves, this can be due to water directly  
398 blocking the stomata. However, in GB most plants have stomata only on the underside of the  
399 leaves, so the transpiration is inhibited by other mechanisms.

400 Physically, the suppression may be due to the fact that energy is used in evaporating the  
401 intercepted water, so less is available for transpiration or that the increased humidity of the air  
402 decreases the evaporative demand (Bosveld and Bouten, 2003). It may also be due to the  
403 presence of water on the leaf surface causing stomatal closure through physiological reactions,  
404 which can be observed even when the stomata are on the underside of a leaf and the water is  
405 lying on the upper side (Ishibashi and Terashima, 1995).

406 In the short term after a rain event, potential water losses due to evaporation may be  
407 underestimated if only potential transpiration is calculated, and therefore overall rates  
408 underestimated. As transpiration is inhibited over the wet fraction of the canopy (Ward and  
409 Robinson, 2000), the PET over a grid box will be a linear combination of the potential  
410 interception and potential transpiration, each weighted by the fraction of the canopy that is wet  
411 or dry. This can be accounted for by introducing an interception term to the calculation of PET,  
412 giving PETI. This is modelled as an interception store, which is (partially) filled by rainfall,  
413 proportionally inhibiting the transpiration. As the interception store dries, the relative  
414 contribution of interception is decreased and the transpiration increases. In this dataset, this  
415 correction is applied on days with precipitation, while on days without precipitation the  
416 potential is equal to the PET defined in Eq. 4. Although an unconventional definition of PET,  
417 a similar interception correction is applied to the PET provided at 40 km resolution by  
418 MORECS (Thompson et al., 1981) which is used widely by hydrologists.

419 This method implicitly assumes that the water is liquid, however snow lying on the canopy will  
420 also inhibit transpiration, and will be depleted by melting as well as by sublimation. The rates  
421 may be slower, and the snow may stay on the canopy for longer than one day. However, the  
422 difference of accounting for canopy snow as distinct from canopy water will have a small effect  
423 on large-scale averages, as the number of days with snow cover in GB is relatively low, and  
424 they occur during winter when the PET is small.

425 The PETI is a weighted sum of the PET,  $E_p$ , (as calculated in Eq 2.) and potential interception,  
426  $E_i$ , which is calculated by substituting zero stomatal resistance,  $r_s=0 \text{ s m}^{-1}$ , into Eq. 4. To  
427 calculate the relative proportions of interception and transpiration, it is assumed that the wet

428 fraction of the canopy is proportional to the amount of water in the interception store. The  
 429 interception store,  $S_I$  ( $\text{kg m}^{-2}$ ), decreases through the day according to an exponential dry down  
 430 (Rutter et al., 1971), such that

$$431 \quad S_I(t) = S_0 e^{-\frac{E_I}{S_{tot}}t}, \quad (13)$$

432 where  $E_I$  is the potential interception,  $S_{tot}$  is the total capacity of the interception store ( $\text{kg m}^{-2}$ ),  
 433  $S_0$  is the precipitation that is intercepted by the canopy ( $\text{kg m}^{-2}$ ) and  $t$  is the time (in days) since  
 434 a rain event. We assume that the interception component is only significant on the day in which  
 435 rainfall occurs, and that it is negligible on subsequent days, so the calculation is only carried  
 436 out for days of non-zero rainfall. Thus  $t$  is a positive fraction between zero and one.

437 The total capacity of the interception store is calculated following Best et al. (2011), such that

$$438 \quad S_{tot} = 0.5 + 0.05\Lambda, \quad (14)$$

439 where  $\Lambda$  is the leaf area index (LAI). For the FAO standard grass land cover the LAI is 2.88  
 440 (Allen et al., 1998). The fraction of precipitation intercepted by the canopy is also found  
 441 following Best et al. (2011), assuming that precipitation lasts for an average of 3 hours.

442 The wet fraction of the canopy,  $C_{wet}$ , is proportional to the store size, such that

$$443 \quad C_{wet}(t) = \frac{S(t)}{S_{tot}}. \quad (15)$$

444 The total PETI is the sum of the interception from the wet canopy and the transpiration from  
 445 the dry canopy,

$$446 \quad E_{PI}(t) = E_I C_{wet}(t) + E_P(1 - C_{wet}(t)). \quad (16)$$

447 This is integrated over one day (from  $t=0$  to  $t=1$ ) to find the total PETI,  $E_{PI}$  ( $\text{mm d}^{-1}$ ), to be

$$448 \quad E_{PI} = S_0 \left(1 - e^{-\frac{E_I}{S_{tot}}}\right) + E_P \left(1 - \frac{S_0}{E_I} \left(1 - e^{-\frac{E_I}{S_{tot}}}\right)\right). \quad (17)$$

449 This calculation is only carried out for days on which rainfall occurs. On subsequent days it is  
 450 assumed that the canopy has sufficiently dried out that the interception component is zero.

451 The PETI is a function of the same six meteorological variables as the PET, plus the  
 452 precipitation.



### 453 **3.2 Spatial and seasonal patterns of PET and PETI**

454 Both PET and PETI have a distinct gradient from low in the north-west to high in the south-  
455 east, and they are both inversely proportional to the elevation (Fig. 6), reflecting the spatial  
456 patterns of the meteorological variables. The PETI is 8 % higher than the PET overall but this  
457 difference is larger in the north and west, where precipitation rates, and therefore interception,  
458 are higher (Fig. 6). In Scotland, the higher interception and lower AED mean that this increase  
459 is a larger proportion of the total, with the mean PETI being 11 % larger than the PET (in some  
460 areas the difference is more than 25%). In the English lowlands the difference is smaller, at 6  
461 %, but this is a more water limited region where hydrological modelling can be sensitive to  
462 even relatively small adjustments to PET (Kay et al., 2013).

463 The seasonal climatology of both PET and PETI follow the meteorology (Fig. 7), with high  
464 values in the summer and low in the winter. Although the relative difference peaks in winter,  
465 the absolute difference between PET and PETI is bimodal, with a peak in March and a smaller  
466 peak in October (September in Scotland) (Fig. 7), because in winter the overall AED is low,  
467 while in summer the amount of precipitation is low, so the interception correction is small. The  
468 seasonal cycle of PET is driven predominantly by the radiative component, which has a much  
469 stronger seasonality than the aerodynamic component (Fig. 8).

470 On a monthly or annual timescale, the ratio of PET to precipitation is an indicator of the wet-  
471 or dryness of a region (Oldekop, 1911; Andréassian et al., 2016). Low values of PET relative  
472 to precipitation indicate wet regions, where evaporation is demand-limited, while high values  
473 indicate dry, water-limited regions. In the wetter regions (Scotland, Wales) mean-monthly PET  
474 and PETI (Fig. 7) are on average lower than the mean-monthly precipitation (Fig. 3) throughout  
475 the year, while in drier regions (England, English lowlands) the mean PET and PETI are higher  
476 than the precipitation for much of the summer, highlighting the regions' susceptibility to  
477 hydrological drought (Folland et al., 2015).

## 478 **4 Decadal trends**

### 479 **4.1 Meteorological Variables**

480 Annual means of the meteorological variables (Fig. 9) and the PET and PETI (Fig. 10) were  
481 calculated for each region. The trends in these annual means were calculated using linear  
482 regression; the significance ( $P$  value) and 95% confidence intervals (CI) of the slope are  
483 calculated specifically allowing for the non-zero lag-1 autocorrelation, to account for possible

484 correlations between adjacent data points (Zwiers and von Storch, 1995; von Storch and Zwiers,  
485 1999). The annual trends can be seen in Table 2. In addition, seasonal means were calculated,  
486 with the four seasons defined to be Winter (December-February), Spring (March-May),  
487 Summer (June-August) and Autumn (September-November), and trends in these means were  
488 also found.

489 The trends in the annual and seasonal means for all regions are plotted in Fig. 11; trends that  
490 are statistically significant at the 5% level are plotted with solid error bars, those that are not  
491 significant are plotted with dashed lines. The analysis was repeated for each pixel in the 1 km  
492 resolution dataset; maps of these rates of change can be seen in Fig. B1.

493 There was a statistically significant trend in air temperature in the English Lowlands throughout  
494 the year. In the other regions the trends were statistically significant in spring and autumn, and  
495 for the annual means. The trends agree with recent trends in the Hadley Centre Central England  
496 Temperature (HadCET) dataset (Parker and Horton, 2005) and in temperature records for  
497 Scotland (Jenkins et al., 2008) as well as in the CRUTEM4 dataset (Jones et al., 2012). An  
498 increase in winter precipitation in Scotland is seen in the current dataset, which leads to a  
499 statistically significant increase in the annual mean precipitation of GB. However, all other  
500 regions and seasons have no statistically significant trends in precipitation. Long term  
501 observations show that there has been little trend in annual precipitation, but a change in  
502 seasonality with wetting winters and drying summers since records began, although with little  
503 change over the past 50 years (Jenkins et al., 2008). The statistically significant decline in wind  
504 speed in all regions is consistent with the results of McVicar et al. (2012) and Vautard et al.  
505 (2010), who report decreasing wind speeds in the northern hemisphere over the late 20<sup>th</sup>  
506 century.

## 507 **4.2 Potential Evapotranspiration**

508 The trends of the meteorological variables are interesting in their own right. But for hydrology,  
509 it is the impact that the trends have on evaporation that matters and that depends on their  
510 combination, which can be expressed through PET.

511 The regional trends of annual mean PET and PETI and the radiative and aerodynamic  
512 components of PET can be seen in Table 2, and the trends in the annual and seasonal means are  
513 plotted in Fig. 12 for all regions. Maps of the trends can be seen in Fig. B2. The trend in the  
514 radiative component of PET is positive over the whole of GB. However, the trend in the

515 aerodynamic component varies; for much of Wales, Scotland and northern England, it is not  
516 significant, or is slightly negative, while in south-east England and north-west Scotland it is  
517 positive. This leads to a positive trend in PET over much of GB, but no significant trend in  
518 southern Scotland and northern England. There is a statistically significant increase in annual  
519 PET in all regions except Wales; the GB trend ( $0.021 \pm 0.021 \text{ mm d}^{-1} \text{ decade}^{-1}$ ) is equivalent to  
520 an increase of  $0.11 \pm 0.11 \text{ mm d}^{-1}$  ( $8.3 \pm 8.1 \%$  of the long term mean) over the whole dataset.  
521 Increases in PETI are only statistically significant in England ( $0.023 \pm 0.023 \text{ mm d}^{-1} \text{ decade}^{-1}$ )  
522 and English lowlands ( $0.028 \pm 0.025 \text{ mm d}^{-1} \text{ decade}^{-1}$ ), where the increases over the whole  
523 dataset are  $0.12 \pm 0.12 \text{ mm d}^{-1}$  ( $8.0 \pm 8.0 \%$  of the long term mean) and  $0.15 \pm 0.13 \text{ mm d}^{-1}$  ( $9.7 \pm 8.8$   
524  $\%$  of the long term mean) respectively. There is a difference in trend between different seasons.  
525 In winter, summer and autumn there are no statistically significant trends in PET or PETI, other  
526 than the English lowlands in autumn, but the spring is markedly different, with very significant  
527 trends ( $P < 0.0005$ ) in all regions. The GB spring trends in PET ( $0.043 \pm 0.019 \text{ mm d}^{-1} \text{ decade}^{-1}$ )  
528 and PETI ( $0.038 \pm 0.018 \text{ mm d}^{-1} \text{ decade}^{-1}$ ) are equivalent to an increase of  $0.22 \pm 0.10 \text{ mm d}^{-1}$   
529 ( $13.8 \pm 6.2 \%$  of the long-term spring mean) and  $0.20 \pm 0.09 \text{ mm d}^{-1}$  ( $11.2 \pm 5.3 \%$  of the long-term  
530 spring mean) over the length of the dataset respectively. The radiative component of PET has  
531 similarly significant trends in spring, while the aerodynamic component has no significant  
532 trends in any season, except the English Lowlands in autumn (Fig. 12).

533 There are few studies of long-term trends in AED in the UK. MORECS provides an estimate  
534 of Penman-Monteith PET with interception correction calculated directly from the 40 km  
535 resolution meteorological data (Hough and Jones, 1997; Thompson et al., 1981), and increases  
536 can be seen over the dataset (Rodda and Marsh, 2011). But as the PET and PETI in the current  
537 dataset are ultimately calculated using the same meteorological data (albeit by different  
538 methods), it is not unexpected that similar trends should be seen. Site-based studies suggest an  
539 increase over recent decades (Burt and Shahgedanova, 1998; Crane and Hudson, 1997), but it  
540 is difficult to separate climate-driven trends from local land-use trends. A global review paper  
541 (McVicar et al., 2012) identified a trend of decreasing AED in the northern hemisphere, driven  
542 by decreasing wind speeds, however they also reported significant local variations on trends in  
543 pan evaporation, including the increasing trend observed by Stanhill and Möller (2008) at a site  
544 in England after 1968. Matsoukas et al. (2011) identified a statistically significant increase in  
545 PET in several regions of the globe, including southern England, between 1983 and 2008,  
546 attributing it predominantly to an increase in the radiative component of PET, due to global  
547 brightening. However, these results were obtained using reanalysis data, which is limited in its

548 ability to capture trends in wind speed. This limitation has been documented in both northern  
549 (Pryor et al., 2009) and southern (McVicar et al., 2008) hemispheres.

550 Regional changes in actual evaporative losses can be estimated indirectly using regional  
551 precipitation and runoff or river flow. Using a combination of observations and modelling,  
552 Marsh and Dixon (2012) identified an increase in evaporative losses in Great Britain from 1961-  
553 2011. Hannaford and Buys (2012) note seasonal and regional differences in trends in observed  
554 river flow, suggesting that decreasing spring flows in the English lowlands are indicative of  
555 increasing AED. However, changing evaporative losses can also be due to changing supply  
556 through precipitation, so it is important to formally attribute the trends in PET to changing  
557 climate, in order to understand changing evapotranspiration.

### 558 **4.3 Attribution of trends in potential evapotranspiration**

559 In order to attribute changes in PET to changes in climate, the rate of change of PET,  $dE_p/dt$   
560 ( $\text{mm d}^{-1} \text{decade}^{-1}$ ), can be calculated as a function of the rate of change of each input variable  
561 (Roderick et al., 2007),

$$562 \frac{dE_p}{dt} = \frac{dE_p}{dT_a} \frac{dT_a}{dt} + \frac{dE_p}{dq_a} \frac{dq_a}{dt} + \frac{dE_p}{du_{10}} \frac{du_{10}}{dt} + \frac{dE_p}{dL_d} \frac{dL_d}{dt} + \frac{dE_p}{dS_d} \frac{dS_d}{dt} . \quad (18)$$

563 Note that we exclude the surface air pressure, because this dataset uses a mean-monthly  
564 climatology as the interannual variability of air pressure is negligible. The derivative of the PET  
565 with respect to each of the meteorological variables can be found analytically (Appendix C).  
566 The derivatives are calculated from the daily meteorological data at 1 km resolution.  
567 Substituting the slopes of the linear regressions of the gridded annual means (Appendix B) for  
568 the rate of change of each variable with time, and the overall time-average of the derivatives of  
569 PET with respect to the meteorological variables, the contribution of each variable to the rate  
570 of change of PET is calculated at 1 km resolution. These are then averaged over the regions of  
571 interest. The same is also applied to the radiative and aerodynamic components independently.

572 Note that this can also be applied to the regional means of the derivatives of PET and the  
573 regional trends in the meteorological variables. The results are compared in Table 3 and the two  
574 approaches are consistent. For the regional analysis, we also quote the 95% CI. However, for  
575 the gridded values, there is such high spatial coherence that combining the 95% CI over the  
576 region results in unreasonably constrained results. We therefore use the more conservative CI  
577 obtained from the regional analysis. Also note that this method assumes that the rate of change

578 of the variables with respect to time is constant over the seasonal cycle (and thus the product of  
579 the means is equal to the mean of the products), and indeed this is how it is often applied  
580 (Donohue et al., 2010; Lu et al., 2016). The effect of this assumption was investigated by  
581 repeating the analysis with seasonal trends and means, but this makes negligible difference to  
582 the results.

583 Figure 13 shows the contribution of each meteorological variable to the rate of change of the  
584 annual mean PET and to the radiative and aerodynamic components and compares the total  
585 attributed trend to that obtained by linear regression. The percentage contribution is in Table 4,  
586 calculated as a fraction of the fitted trend. The final column shows the total attributed trend (i.e.  
587 the sum of the previous columns) as a percentage of the fitted trend, to demonstrate the success  
588 of the attribution at recovering the fitted trends. For the PET trend and for the trend in the  
589 radiative component, these values generally sum to the linear regression to within a few percent.  
590 However, for the aerodynamic component, the fitted trends are much smaller than the statistical  
591 uncertainty. This means that there can be a large and/or negative percentage difference between  
592 the attributed and fitted trends, even when the absolute difference is negligible.

593 The largest overall contribution to the rate of change of PET comes from increasing air  
594 temperature, which has the effect of increasing the aerodynamic component but decreasing the  
595 radiative component. The latter effect is due to approximating the surface temperature with the  
596 air temperature in the calculation of upwelling LW radiation. This assumption is applied as it  
597 simplifies the surface energy balance but it may introduce artefacts into the calculation of PET.  
598 A more thorough formulation of PET, which linearises the net radiation in the derivation of the  
599 Penman-Monteith equation, can be calculated to allow for a non-negligible difference between  
600 air and surface temperature (Monteith, 1981; Thompson et al., 1981), but the difference  
601 between the more thorough formulation and the formulation used here is small, particularly for  
602 the temperature range of GB.

603 Note that in this calculation we are assuming that air temperature and downward LW radiation  
604 vary independently, while in reality (and implicit in the calculation of downward LW in Sect.  
605 2.4), downward LW radiation is also a function of the air temperature so that increases in  
606 downward LW may broadly cancel the increasing upwelling LW radiation. If we instead were  
607 to use net LW radiation as the independent variable, it is likely that dependence of the rate of  
608 change of the radiative component on air temperature would be reduced in magnitude and  
609 compensated by the rate of change of net LW radiation.

610 Overall the next largest increases are caused by increasing downward SW radiation, particularly  
611 in the English regions in the spring, as it increases the radiative component of PET. However,  
612 in Scotland and Wales, the increasing downward LW radiation is also important. Increasing  
613 specific humidity strongly decreases the PET by decreasing the aerodynamic component, while  
614 the decreasing wind speed has the effect of increasing the radiative component, but more  
615 strongly decreasing the aerodynamic component, so overall it tends to cause a decrease in PET.  
616 Since the increasing air temperature and downward LW and SW radiation have the effect of  
617 increasing PET, but the increasing specific humidity and decreasing wind speed tend to  
618 decrease it, then the overall trend is positive, but smaller than the trend due to air temperature  
619 alone.

#### 620 **4.4 Relative humidity**

621 The increase in PET due to increasing air temperature is largely cancelled by the decrease due  
622 to increasing specific humidity so that the overall trend is smaller than the contribution to the  
623 increase from air temperature alone. However, although we have assumed that specific  
624 humidity and air temperature are independent variables, they are in fact coevolving in a  
625 warming atmosphere. As air temperature increases, the saturated specific humidity increases  
626 according to the Clausius-Clapeyron relation (Schneider et al., 2010). However, since  
627 evaporation also increases with rising temperature, the increased water flux into the atmosphere  
628 ensures that specific humidity also increases and it can be shown that there is likely to be little  
629 change in global relative humidity even with significant change in global temperature (Held  
630 and Soden, 2006; Schneider et al., 2010), although this may vary regionally over land (Dai,  
631 2006). Although it is not completely independent of air temperature, an alternative way of  
632 assessing the drivers of AED is to consider relative humidity,  $R_h$ , as the independent humidity  
633 variable. In this case, the PET can be recast in terms of relative humidity, such that

$$634 \quad E_P = \frac{t_d}{\lambda} \frac{\Delta A + \frac{c_p \rho_a}{r_a} q_s (1 - R_h)}{\Delta + \gamma \left(1 + \frac{r_s}{r_a}\right)}. \quad (19)$$

635 Relative humidity is calculated from the specific humidity using

$$636 \quad R_h = \frac{q_a}{q_s}. \quad (20)$$

637 Although in this case relative humidity is a function of air temperature, through the saturated  
638 specific humidity, in reality they are often found to behave as independent variables. It has been

639 shown that there is little cancellation of the air temperature and relative humidity terms when  
640 studying both historical data and future climate projections (Scheff and Frierson, 2014).

641 The relative humidity annual means, mean-monthly climatology and seasonal trends can be  
642 seen in Fig. 14. We find a statistically significant negative trend in relative humidity in the  
643 spring and autumn (except Wales in the autumn) but no overall negative trend in winter or  
644 summer and no significant trend in the annual means. Maps of the overall mean relative  
645 humidity and the trend in the annual mean are in Fig B3. There are only small regions in the  
646 west of Scotland and the east and south west of England where there are significant trends in  
647 the annual mean.

648 We calculate an alternative attribution using relative humidity as a variable, rather than specific  
649 humidity, such that

$$650 \frac{dE_p}{dt} = \frac{dE_p}{dT_a} \frac{dT_a}{dt} + \frac{dE_p}{dR_h} \frac{dR_h}{dt} + \frac{dE_p}{du_{10}} \frac{du_{10}}{dt} + \frac{dE_p}{dL_d} \frac{dL_d}{dt} + \frac{dE_p}{dS_d} \frac{dS_d}{dt} . \quad (21)$$

651 We then calculate the derivative of the PET with respect to relative humidity and the derivatives  
652 with respect to air temperature and pressure are now taken at constant  $R_h$  rather than constant  
653  $q_a$ , so these are also recalculated. See Appendix C for details.

654 Figure 15 shows the contribution of the different variables to the rate of change of PET with  
655 this alternative formulation. The total attributed change is nearly the same as that in Fig. 13,  
656 although there are small differences due to statistical uncertainty in the fits. The contributions  
657 of downward SW and LW radiation and of wind speed to the rate of change of PET are  
658 unchanged. Although it is not statistically significant, the negative trend in relative humidity  
659 leads to an increase in the aerodynamic component, which is larger than the increase due to  
660 increasing downward SW radiation. The contribution of air temperature to the rate of change  
661 is significantly reduced compared to the specific humidity formulation. The air temperature-  
662 driven decrease in the radiative component now largely cancels the temperature-driven increase  
663 in the aerodynamic component, which is much smaller than in Sect. 4.3 as it now implicitly  
664 includes the rising specific humidity. However, the effect of air temperature on the radiative  
665 component comes through the effect of air temperature on the upwelling LW radiation in the  
666 calculation of net radiation and this is dependent on the simplifying assumption that the surface  
667 temperature is equal to the air temperature when solving the energy balance. If the fully  
668 linearised version of the Penman-Monteith equation were used (Monteith, 1981), then the  
669 dependence on air temperature would be more complicated as it would account for a non-

670 negligible difference between air and surface temperature. This may result in a different  
671 contribution of air temperature to the changing PET, although this difference is likely to be  
672 small.

## 673 **5 Discussion**

674 These high resolution datasets provide insight into the effect of the changing climate of Great  
675 Britain on AED over the past five decades. There have been significant climatic trends in the  
676 UK since 1961; in particular rising air temperature and specific humidity, decreasing wind  
677 speed and decreasing cloudiness. Although some are positive and some negative, these  
678 meteorological trends combine to give statistically significant trends in PET.

679 Wind speeds have decreased more significantly in the west than the east, and show a consistent  
680 decrease across seasons. Contrary to Donohue et al. (2010) and McVicar et al. (2012), this study  
681 finds that the change in wind speed of the late 20<sup>th</sup> and early 21<sup>st</sup> centuries has not had a  
682 dominant influence on PET over the period of study, although it has mitigated the increasing  
683 trend in PET. However, the previous studies were concerned with open-water Penman  
684 evaporation, which has a simpler (proportional) dependence on wind speed than the Penman-  
685 Monteith PET considered here (Schymanski and Or, 2015).

686 The air temperature trend in this study of  $0.21 \pm 0.15$  K decade<sup>-1</sup> in GB is consistent with  
687 observed global and regional trends (Hartmann et al., 2013; Jenkins et al., 2008). The  
688 temperature trend is responsible for a large contribution to the trend in PET, although the large  
689 negative contribution from the specific humidity (as well as a small negative contribution from  
690 wind speed) means that the overall trend is smaller than the temperature trend alone.

691 When the attribution is recast in terms of relative humidity, the effect of air temperature is much  
692 smaller, supporting the hypothesis that the temperature and specific humidity components  
693 cancel because their changes are part of the same thermodynamic warming processes. Much of  
694 the increase in the aerodynamic component due to air temperature is cancelled by the decrease  
695 of the radiative component, which is due to the effect of air temperature on the calculated  
696 upwelling LW radiation. However this is because of the assumption that surface temperature  
697 can be approximated with air temperature, thus the real physical contribution of air temperature  
698 in the relative humidity formulation is likely to be roughly equal to the increase in the  
699 aerodynamic component. Although the relative humidity does not have a statistically significant  
700 trend overall (although there are significant trends in spring and for some regions in autumn),  
701 it is large enough that the negative trend in relative humidity is the largest contribution to the



702 increasing PET, followed by the downward SW radiation. This corresponds well to recent  
703 findings in Spain (Vicente-Serrano et al., 2016).

704 The trend in relative humidity is consistent with that seen in historical regional (Jenkins et al.,  
705 2008) and global (Dai, 2006; Willett et al., 2014) analyses. Although not statistically significant  
706 overall, it contributes to between 57 % and 68 % of the trends in PET (between 39 % and 46 %  
707 or the trends in spring PET). Globally trends in relative humidity vary spatially, with mid-  
708 latitudes showing a decrease and the tropics and high-latitudes showing an increase, despite an  
709 overall increase in specific humidity over land, particularly in the Northern Hemisphere (Dai,  
710 2006; Willett et al., 2014). In these global analyses, Great Britain is in a region of transition  
711 between decreasing relative humidity in Western Europe and increasing relative humidity in  
712 Scandinavia, so that small decreasing trends are found, but they are not significant; this is  
713 consistent with our findings. We found the relative humidity to be decreasing significantly in  
714 spring, which is also when the downward SW is increasing. This is consistent with reduced  
715 precipitation and cloud cover due to changing weather patterns (Sutton and Dong, 2012).

716 Increasing solar radiation has been shown to increase spring and annual AED, contributing to  
717 between 18 % and 50 % of the fitted trend in annual PET, and to between 43 % and 53 % of  
718 the fitted trend in spring PET. Two main mechanisms can be responsible for changing solar  
719 radiation: changing cloud cover and changing aerosol concentrations. Changing aerosol  
720 emissions have been shown to have had a significant effect on solar radiation in the 20<sup>th</sup> century.  
721 In Europe, global dimming due to increased aerosol concentrations peaked around 1980,  
722 followed by global brightening as aerosol concentrations decreased (Wild, 2009). Observations  
723 of changing continental runoff and river flow in Europe over the 20<sup>th</sup> century have been  
724 attributed to changing aerosol concentrations, via their effect on solar radiation, and thus AED  
725 (Gedney et al., 2014).

726 In this study we use the duration of bright sunshine to calculate the solar radiation, using  
727 empirical coefficients which do not vary with year, so aerosol effects are not explicitly included  
728 and the trend in downward SW is driven by the increase in sunshine hours in the MORECS  
729 dataset ( $0.088 \pm 0.055 \text{ h d}^{-1} \text{ decade}^{-1}$  over GB). The coefficients used in this study to convert  
730 sunshine hours to radiation fluxes were empirically derived in 1978; the derivation used data  
731 from the decade 1966-75, as this period was identified to be before reductions in aerosol  
732 emissions had begun to significantly alter observed solar radiation (Cowley, 1978). Despite  
733 this, the trend in SW radiation in the current dataset from 1979 onwards ( $1.4 \pm 1.4 \text{ W m}^{-2} \text{ decade}^{-1}$ )

734 <sup>1</sup>) is consistent, within uncertainties, with that seen over GB in the WFDEI data ( $0.9 \pm 1.1 \text{ W m}^{-2}$   
735  $\text{decade}^{-1}$ ), which is bias-corrected to observations and includes explicit aerosol effects  
736 (Weedon et al., 2014).

737 It has been suggested that aerosol effects also implicitly affect sunshine duration since in  
738 polluted areas there will be fewer hours above the official ‘sunshine hours’ threshold of  $120$   
739  $\text{Wm}^{-2}$  (Helmes and Jaenicke, 1986). Several regional studies have shown trends in sunshine  
740 hours that are consistent with the periods of dimming and brightening across the globe (eg  
741 Liley, 2009; Sanchez-Lorenzo et al., 2009; Sanchez-Lorenzo et al., 2008; Stanhill and Cohen,  
742 2005), and several have attempted to quantify the relative contribution of trends in cloud cover  
743 and aerosol loading (e.g. Sanchez-Lorenzo and Wild (2012) in Switzerland, see Sanchez-  
744 Romero et al. (2014) for a review). Therefore, it may be that some of the brightening trend seen  
745 in the current dataset is due to the implicit signal of aerosol trends in the MORECS sunshine  
746 duration, although this is likely to be small compared to the effects of changing cloud cover.

747 The trends in the MORECS sunshine duration used in this study are consistent with changing  
748 weather patterns which may be attributed to the Atlantic Multidecadal Oscillation (AMO). The  
749 AMO has been shown to cause a decrease in spring precipitation (and therefore cloud cover) in  
750 northern Europe over recent decades (Sutton and Dong, 2012), and the trend in MORECS  
751 sunshine hours is dominated by an increase in the spring mean. This has also been seen in  
752 Europe-wide sunshine hours data (Sanchez-Lorenzo et al., 2008) and is also consistent with the  
753 falling spring relative humidity found in the current study. On the other hand, the effect of  
754 changing aerosols on sunshine hours is expected to be largest in the winter (Sanchez-Lorenzo  
755 et al., 2008). However, it would not be possible to directly identify either of these effects on the  
756 sunshine duration without access to longer data records.

757 The inclusion of explicit aerosol effects in the coefficients of the Ångström-Prescott equation  
758 would be expected to reduce the positive trend in AED in the first two decades of the dataset,  
759 and increase it after 1980. Gedney et al. (2014) attribute a decrease in European solar radiation  
760 of  $10 \text{ W m}^{-2}$  between the periods 1901-10 and 1974-80, and an increase of  $4 \text{ W m}^{-2}$  from 1974-  
761 84 to 1990-99 to changing aerosol contributions. Applying these trends to the current dataset,  
762 with a turning point at 1980, would double the overall increase in solar radiation in Great  
763 Britain, which would lead to a 40 % increase in the overall trend in PET. So, if this effect were  
764 to be included, it would confirm the results found in this paper.

765 Although the contribution is generally smaller (except in Scotland), the trends in LW radiation  
766 in these datasets contribute to between 15% and 27% of the trends in PET and between 27%  
767 and 46% of the trends in the radiative component. In Scotland the downward LW radiation is  
768 the dominant driver of changing PET in the relative humidity formulation. Note, however, that  
769 this is largely cancelled by the increasing upwelling LW, which is captured in this study in the  
770 effect of air temperature on the radiative component, and which may be different if the  
771 approximation that the difference between air temperature and surface temperature is negligible  
772 were relaxed. Observations of LW radiation are often uncertain, but the trend in this dataset,  
773 although small, is consistent with observed trends (Wang and Liang, 2009), as well as with  
774 trends in the WFDEI bias-corrected reanalysis product (Weedon et al., 2014).

775 Trends in temperature and cloud cover in the UK are expected to continue into the coming  
776 decades, with precipitation expected to increase in the winter but decrease in the summer  
777 (Murphy et al., 2009). Therefore it is likely that AED will increase, increasing water stress in  
778 the summer when precipitation is lower and potentially affecting water resources, agriculture  
779 and biodiversity. This has been demonstrated for southern England and Wales by Rudd and  
780 Kay (2015), who calculated present and future PET using high-resolution RCM output and  
781 included the effects of CO<sub>2</sub> on stomatal opening.

782 The current study is concerned only with the effects of changing climate on AED and has  
783 assumed a constant bulk canopy resistance throughout. However, plants are expected to react  
784 to increased CO<sub>2</sub> in the atmosphere by closing stomata and limiting the exchange of gases,  
785 including water (Kruijt et al., 2008), and observed changes in runoff have been attributed to this  
786 effect (Gedney et al., 2006; Gedney et al., 2014). It is possible that the resulting change of  
787 canopy resistance could partially offset the increased atmospheric demand (Rudd and Kay,  
788 2015) and may impact runoff (Gedney et al., 2006; Prudhomme et al., 2014), but further studies  
789 would be required to quantify this.

## 790 **6 Conclusion**

791 This paper has presented a unique, high-resolution, observation-based dataset of meteorological  
792 variables and AED in Great Britain since 1961. Key trends in the meteorological variables are  
793 (i) increasing air temperature and specific humidity, consistent with global temperature trends;  
794 (ii) increasing solar radiation, particularly in the spring, consistent with changes in aerosol  
795 emissions and weather patterns in recent decades; (iii) decreasing wind speed, consistent with  
796 observations of global stilling; (iv) increasing precipitation, driven by increasing winter

797 precipitation in Scotland; and (v) no significant trend in relative humidity overall, but  
798 decreasing relative humidity in the spring. The meteorological variables were used to evaluate  
799 AED in Great Britain via calculation of PET and PETI. It has been demonstrated that including  
800 the interception component in the calculation of PETI gives a mean estimate that is overall 8%  
801 larger than PET alone, with strong seasonality and spatial variation of the difference. PET was  
802 found to be increasing by  $0.021 \pm 0.021 \text{ mm d}^{-1} \text{ decade}^{-1}$  in GB over the study period. With the  
803 interception component included, the trend in PETI is weaker ( $0.019 \pm 0.020 \text{ mm d}^{-1}$ ), and over  
804 GB is not significant at the 5% level. The trend in PET was analytically attributed to the trends  
805 in the meteorological variables, and it was found that the dominant effect was that increasing  
806 air temperature was driving increasing PET, with smaller increases from increased downward  
807 SW and LW radiation. However, the effect of temperature is largely compensated by the  
808 associated increase in specific humidity, while decreasing wind speed tended to decrease the  
809 PET. When the attribution was recast in terms of relative humidity, temperature was found to  
810 have a small effect on the trend in PET due to cancellation between the increase in the  
811 aerodynamic component and decrease in the radiative component, while the decreasing relative  
812 humidity caused PET to increase, at a similar rate to the downward SW radiation (and  
813 downward LW radiation in Scotland). The increase in PET due to these variables is mitigated  
814 by the observed northern hemisphere wind stilling, which causes a decrease in PET, however,  
815 the overall trend in PET is positive over the period of study.

816 In addition to providing meteorological data and estimates of AED for analysis, the  
817 meteorological variables provided are sufficient to run LSMs and hydrological models. The  
818 high spatial (1 km) and temporal (daily) resolution will allow this dataset to be used to study  
819 the effects of climate on physical and biological systems at a range of scales, from local to  
820 national.

## 821 **Data Access**

822 The data can be downloaded from the Environmental Information Platform at the Centre for  
823 Ecology & Hydrology. The meteorological variables (CHESS-met) can be found at  
824 <https://catalogue.ceh.ac.uk/documents/80887755-1426-4dab-a4a6-250919d5020c>,  
825 while the PET and PETI (CHESS-PE) can be accessed at  
826 <https://catalogue.ceh.ac.uk/documents/d329f4d6-95ba-4134-b77a-a377e0755653>.

## 827 **Author contribution**

828 EB, JF and DBC designed the study. JF, ACR, DBC and ELR developed code to create  
829 meteorological data. ELR created the PET and PETI. ELR and EB analysed trends. ELR, EB,  
830 ACR and DBC wrote the manuscript.

### 831 **Acknowledgements**

832 The meteorological variables presented are based largely on GB meteorological data under  
833 licence from the Met Office, and those organisations contributing to this national dataset  
834 (including the Met Office, Environment Agency, Scottish Environment Protection Agency  
835 (SEPA) and Natural Resources Wales) are gratefully acknowledged. The CRU TS 3.21 daily  
836 temperature range data were created by the University of East Anglia Climatic Research Unit,  
837 and the WFD air pressure data were created as part of the EU FP6 project WATCH (Contract  
838 036946). Collection of flux data was funded by EU FP4 EuroFlux (Griffin Forest); EU FP5  
839 CarboEuroFlux (Griffin Forest); EU FP5 GreenGrass (Easter Bush); EU FP6 CarboEuropeIP  
840 (Alice Holt , Griffin Forest, Auchencorth Moss, Easter Bush); EU FP6 IMECC (Griffin  
841 Forest); the Forestry Commission (Alice Holt); the Natural Environment Research Council,  
842 UK (Auchencorth Moss, Easter Bush).

843 Fig. 1, panels a) and b) of Fig. 6 and panel a) of Fig. B3 were produced with the python  
844 implementation of the cubehelix colour scheme (Green, 2011).

845 Thanks to Nicola Gedney and Graham Weedon for useful discussions.

846 Thanks to three anonymous reviewers, who provided insightful and helpful comments.

847 This work was partially funded by the Natural Environment Research Council in the  
848 Changing Water Cycle programme: NERC Reference: NE/I006087/1.

849

## 850 **Appendix A: Data validation**

851 Meteorological data were downloaded from the European Fluxes Database Cluster  
852 (<http://gaia.agraria.unitus.it>) for four sites positioned around Great Britain. Two were woodland  
853 sites (Alice Holt (Wilkinson et al., 2012; Heinemeyer et al., 2012) and Griffin Forest (Clement,  
854 2003)), while two had grass and crop cover (Auchencorth Moss (Billett et al., 2004) and Easter  
855 Bush (Gilmanov et al., 2007; Soussana et al., 2007)). Table A1 gives details of the data used.  
856 The data are provided as half-hourly measurements, which were used to create daily means,  
857 where full daily data coverage was available. The daily means of the observed data were  
858 compared to the daily data from the grid square containing the site and the Pearson correlation  
859 ( $r^2$ ), mean bias and root mean square error (RMSE) were calculated. For each site, monthly  
860 means were calculated where the full month had available data, then a climatology calculated  
861 from available months. The same values were calculated from the relevant grid squares, using  
862 only time periods for which observed data were available.

863 Fig. A1 shows the comparison of the data set downward SW radiation against daily mean air  
864 temperature observed at the four sites. Fig. A2 shows the mean-monthly climatology of the  
865 daily values. The observed values of the mixing ratio of water vapour in air were compared  
866 with values calculated from the meteorological dataset, using the equation

$$867 \quad r_w = q_a \left( \frac{m_a}{m_w} \right) \quad (\text{A1})$$

868 where  $m_a$  is the molecular mass of dry air and  $m_w$  is the molecular mass of water. The  
869 comparisons are shown in Figs. A3 and A4.

870 Table A2 shows the  $r^2$ , mean bias and RMSE for each of the variables included in the validation  
871 exercise. The correlations indicate a good relationship between the dataset variables and the  
872 independent observations at the sites, while the mean-monthly climatologies demonstrate that  
873 the data represent the seasonal cycle well. The data set downward SW in Auchencorth Moss is  
874 biased high compared to the observations, while the wind speed is biased high at two sites.

## 875 **Appendix B: Trend maps**

876 Fig. B1 shows the rate of change of each of the meteorological variables at the 1 km resolution,  
877 while Fig. B2 shows the rate of change of the PET, PETI, and the two components of PET at  
878 the same resolution. This shows that the regional trends are consistent with spatial variation and  
879 are not dominated by individual extreme points.

880 **Appendix C: Derivatives of PET**

881 The wind speed affects the PET through the aerodynamic resistance. The derivative with respect  
882 to wind speed is

$$883 \quad \frac{\partial E_P}{\partial u_{10}} = \frac{(\Delta + \gamma)E_{PA} - \gamma \frac{T_s}{r_a} E_{PR}}{u_{10} \left( \Delta + \gamma \left( 1 + \frac{r_s}{r_a} \right) \right)}. \quad (C1)$$

884 The downward LW and SW radiation affect PET through the net radiation, and the derivatives  
885 are

$$886 \quad \frac{\partial E_P}{\partial L_d} = E_{PR} \frac{\epsilon}{R_n} \quad (C2)$$

$$887 \quad \frac{\partial E_P}{\partial S_d} = E_{PR} \frac{(1 - \alpha)}{R_n}. \quad (C3)$$

888 The derivative of PET with respect to specific humidity is

$$889 \quad \frac{\partial E_P}{\partial q_a} = \frac{E_{PA}}{q_a - q_s}. \quad (C4)$$

890 The air temperature affects PET through the saturated specific humidity and its derivative, the  
891 net radiation and the air density, so that the derivative of PET with respect to air temperature is

$$892 \quad \frac{\partial E_P}{\partial T_a} = E_{PR} \left[ \left( 1 - \frac{\Delta}{\Delta + \gamma \left( 1 + \frac{r_s}{r_a} \right)} \right) \left( \frac{T_{sp}}{T_a^2} \frac{\sum_{i=1}^4 i(i-1) a_i T_r^{i-2}}{\sum_{i=1}^4 i a_i T_r^{i-1}} + \Delta \frac{p_* + (1 - \epsilon) e_s}{p_* q_s} - \frac{2}{T_a} \right) - \frac{4 \epsilon \sigma T_a^3}{R_n} \right] +$$

$$893 \quad E_{PA} \left[ \frac{\Delta}{q_s - q_a} - \frac{1}{T_a} - \frac{\Delta}{\Delta + \gamma \left( 1 + \frac{r_s}{r_a} \right)} \left( \frac{T_{sp}}{T_a^2} \frac{\sum_{i=1}^4 i(i-1) a_i T_r^{i-2}}{\sum_{i=1}^4 i a_i T_r^{i-1}} + \Delta \frac{p_* + (1 - \epsilon) e_s}{p_* q_s} - \frac{2}{T_a} \right) \right]. \quad (C5)$$

894 When calculating the attribution with relative humidity as the dependent variable, the derivative  
895 of PET with respect to relative humidity is

$$896 \quad \frac{\partial E_P}{\partial R_h} = \frac{E_{PA}}{R_h - 1}, \quad (C6)$$

897 and the derivative of PET with respect to air temperature is

$$898 \quad \frac{\partial E_P}{\partial T_a} = E_{PR} \left[ \left( 1 - \frac{\Delta}{\Delta + \gamma \left( 1 + \frac{r_s}{r_a} \right)} \right) \left( \frac{T_{sp}}{T_a^2} \frac{\sum_{i=1}^4 i(i-1) a_i T_r^{i-2}}{\sum_{i=1}^4 i a_i T_r^{i-1}} + \Delta \frac{p_* + (1 - \epsilon) e_s}{p_* q_s} - \frac{2}{T_a} \right) - \frac{4 \epsilon \sigma T_a^3}{R_n} \right] +$$

$$899 \quad E_{PA} \left[ \frac{\Delta}{q_s} - \frac{1}{T_a} - \frac{\Delta}{\Delta + \gamma \left( 1 + \frac{r_s}{r_a} \right)} \left( \frac{T_{sp}}{T_a^2} \frac{\sum_{i=1}^4 i(i-1) a_i T_r^{i-2}}{\sum_{i=1}^4 i a_i T_r^{i-1}} + \Delta \frac{p_* + (1 - \epsilon) e_s}{p_* q_s} - \frac{2}{T_a} \right) \right]. \quad (C7)$$

900 The difference between Eq. C7 and Eq. C5 is the factor of  $\Delta/q_s$  instead of  $\Delta/(q_s - q_a)$  in the  
901 second bracket.

## 902 7 References

- 903 Allen, R. G., Pereira, L. S., Raes, D., and Smith, M.: Crop evapotranspiration - Guidelines for  
904 computing crop water requirements, Food and Agriculture Organization of the United  
905 Nations, Rome, Italy, FAO Irrigation and Drainage Paper, 1998.
- 906 Allen, R. G., Trezza, R., and Tasumi, M.: Analytical integrated functions for daily solar  
907 radiation on slopes, *Agricultural and Forest Meteorology*, 139, 55-73,  
908 doi:10.1016/j.agrformet.2006.05.012, 2006.
- 909 Andréassian, V., Mander, Ü., and Pae, T.: The Budyko hypothesis before Budyko: The  
910 hydrological legacy of Evald Oldekop, *Journal of Hydrology*, 535, 386-391,  
911 <http://dx.doi.org/10.1016/j.jhydrol.2016.02.002>, 2016.
- 912 Ångström, A.: A study of the radiation of the atmosphere, *Smithsonian Miscellaneous*  
913 *Collections*, 65, 159-161, 1918.
- 914 Azizzadeh, M., and Javan, K.: Analyzing Trends in Reference Evapotranspiration in  
915 Northwest Part of Iran, *Journal of Ecological Engineering*, 16, 1-12,  
916 10.12911/22998993/1853, 2015.
- 917 Baldocchi, D., Valentini, R., Running, S., Oechel, W., and Dahlman, R.: Strategies for  
918 measuring and modelling carbon dioxide and water vapour fluxes over terrestrial ecosystems,  
919 *Global Change Biology*, 2, 159-168, doi:10.1111/j.1365-2486.1996.tb00069.x, 1996.
- 920 Bell, V. A., Kay, A. L., Jones, R. G., Moore, R. J., and Reynard, N. S.: Use of soil data in a  
921 grid-based hydrological model to estimate spatial variation in changing flood risk across the  
922 UK, *Journal of Hydrology*, 377, 335-350, doi:10.1016/j.jhydrol.2009.08.031, 2009.
- 923 Bell, V. A., Gedney, N., Kay, A. L., Smith, R. N. B., Jones, R. G., and Moore, R. J.:  
924 Estimating Potential Evaporation from Vegetated Surfaces for Water Management Impact  
925 Assessments Using Climate Model Output, *J Hydrometeorol*, 12, 1127-1136,  
926 doi:10.1175/2011jhm1379.1, 2011.
- 927 Bell, V. A., Kay, A. L., Cole, S. J., Jones, R. G., Moore, R. J., and Reynard, N. S.: How might  
928 climate change affect river flows across the Thames Basin? An area-wide analysis using the  
929 UKCP09 Regional Climate Model ensemble, *Journal of Hydrology*, 442-443, 89-104,  
930 doi:10.1016/j.jhydrol.2012.04.001, 2012.
- 931 Bellamy, P. H., Loveland, P. J., Bradley, R. I., Lark, R. M., and Kirk, G. J.: Carbon losses  
932 from all soils across England and Wales 1978-2003, *Nature*, 437, 245-248,  
933 doi:10.1038/nature04038, 2005.
- 934 Berry, P. M., Dawson, T. P., Harrison, P. A., and Pearson, R. G.: Modelling potential impacts  
935 of climate change on the bioclimatic envelope of species in Britain and Ireland, *Global*  
936 *Ecology and Biogeography*, 11, 453-462, doi:10.1046/j.1466-822x.2002.00304.x, 2002.
- 937 Best, M. J., Pryor, M., Clark, D. B., Rooney, G. G., Essery, R. L. H., Ménard, C. B., Edwards,  
938 J. M., Hendry, M. A., Porson, A., Gedney, N., Mercado, L. M., Sitch, S., Blyth, E., Boucher,  
939 O., Cox, P. M., Grimmond, C. S. B., and Harding, R. J.: The Joint UK Land Environment  
940 Simulator (JULES), model description – Part 1: Energy and water fluxes, *Geoscientific Model*  
941 *Development*, 4, 677-699, doi:10.5194/gmd-4-677-2011, 2011.
- 942 Billett, M. F., Palmer, S. M., Hope, D., Deacon, C., Storeton-West, R., Hargreaves, K. J.,  
943 Flechard, C., and Fowler, D.: Linking land-atmosphere-stream carbon fluxes in a lowland  
944 peatland system, *Global Biogeochemical Cycles*, 18, n/a-n/a, 10.1029/2003gb002058, 2004.



- 945 Bosveld, F. C., and Bouten, W.: Evaluating a Model of Evaporation and Transpiration with  
946 Observations in a Partially Wet Douglas-Fir Forest, *Boundary-Layer Meteorology*, 108, 365-  
947 396, 10.1023/a:1024148707239, 2003.
- 948 Burch, S. F., and Ravenscroft, F.: Computer modelling of the UK wind energy resource: Final  
949 overview report., AEA Industrial Technology, 1992.
- 950 Burt, T. P., and Shahgedanova, M.: An historical record of evaporation losses since 1815  
951 calculated using long-term observations from the Radcliffe Meteorological Station, Oxford,  
952 England, *Journal of Hydrology*, 205, 101-111, doi:10.1016/S0022-1694(97)00143-1, 1998.
- 953 Clark, D. B., Mercado, L. M., Sitch, S., Jones, C. D., Gedney, N., Best, M. J., Pryor, M.,  
954 Rooney, G. G., Essery, R. L. H., Blyth, E., Boucher, O., Harding, R. J., Huntingford, C., and  
955 Cox, P. M.: The Joint UK Land Environment Simulator (JULES), model description – Part 2:  
956 Carbon fluxes and vegetation dynamics, *Geoscientific Model Development*, 4, 701-722,  
957 doi:10.5194/gmd-4-701-2011, 2011.
- 958 Clement, R. M., J.B.; Jarvis, P.G.: Net carbon productivity of Sitka Spruce forest in Scotland,  
959 *Scottish Forestry*, 5-10, 2003.
- 960 Cowley, J. P.: The distribution over Great Britain of global solar irradiation on a horizontal  
961 surface, *Meteorological Magazine*, 107, 357-372, 1978.
- 962 Crane, S. B., and Hudson, J. A.: The impact of site factors and climate variability on the  
963 calculation of potential evaporation at Moel Cynnedd, Plynlimon, *Hydrol. Earth Syst. Sci.*, 1,  
964 429-445, doi:10.5194/hess-1-429-1997, 1997.
- 965 Crooks, S. M., and Naden, P. S.: CLASSIC: a semi-distributed rainfall-runoff modelling  
966 system, *Hydrol. Earth Syst. Sci.*, 11, 516-531, doi:10.5194/hess-11-516-2007, 2007.
- 967 Crooks, S. M., and Kay, A. L.: Simulation of river flow in the Thames over 120 years:  
968 Evidence of change in rainfall-runoff response?, *Journal of Hydrology: Regional Studies*, 4,  
969 Part B, 172-195, doi:10.1016/j.ejrh.2015.05.014, 2015.
- 970 Dai, A.: Recent Climatology, Variability, and Trends in Global Surface Humidity, *Journal of*  
971 *Climate*, 19, 3589-3606, doi:10.1175/JCLI3816.1, 2006.
- 972 Dilley, A. C., and O'Brien, D. M.: Estimating downward clear sky long-wave irradiance at the  
973 surface from screen temperature and precipitable water, *Quarterly Journal of the Royal*  
974 *Meteorological Society*, 124, 1391-1401, doi:10.1256/Smsqj.54902, 1998.
- 975 Donohue, R. J., McVicar, T. R., and Roderick, M. L.: Assessing the ability of potential  
976 evaporation formulations to capture the dynamics in evaporative demand within a changing  
977 climate, *Journal of Hydrology*, 386, 186-197, doi:10.1016/j.jhydrol.2010.03.020, 2010.
- 978 Doorenbos, J. a. P., W. O.: Crop water requirements. FAO Irrigation and Drainage Paper 24.,  
979 FAO, Rome, Italy, 1977.
- 980 Evans, N., Baierl, A., Semenov, M. A., Gladders, P., and Fitt, B. D.: Range and severity of a  
981 plant disease increased by global warming, *Journal of the Royal Society, Interface / the Royal*  
982 *Society*, 5, 525-531, doi:10.1098/rsif.2007.1136, 2008.
- 983 FAO/IIASA/ISRIC/ISS-CAS/JRC: Harmonized World Soil Database, 2012.
- 984 Field, M.: The meteorological office rainfall and evaporation calculation system —  
985 MORECS, *Agricultural Water Management*, 6, 297-306, [http://dx.doi.org/10.1016/0378-  
986 3774\(83\)90017-3](http://dx.doi.org/10.1016/0378-3774(83)90017-3), 1983.

- 987 Fleig, A. K., Tallaksen, L. M., James, P., Hisdal, H., and Stahl, K.: Attribution of European  
988 precipitation and temperature trends to changes in synoptic circulation, *Hydrology and Earth  
989 System Sciences*, 19, 3093-3107, 10.5194/hess-19-3093-2015, 2015.
- 990 Folland, C. K., Hannaford, J., Bloomfield, J. P., Kendon, M., Svensson, C., Marchant, B. P.,  
991 Prior, J., and Wallace, E.: Multi-annual droughts in the English Lowlands: a review of their  
992 characteristics and climate drivers in the winter half-year, *Hydrology and Earth System  
993 Sciences*, 19, 2353-2375, doi:10.5194/hess-19-2353-2015, 2015.
- 994 Gedney, N., Cox, P. M., Betts, R. A., Boucher, O., Huntingford, C., and Stott, P. A.:  
995 Detection of a direct carbon dioxide effect in continental river runoff records, *Nature*, 439,  
996 835-838, doi:10.1038/nature04504, 2006.
- 997 Gedney, N., Huntingford, C., Weedon, G. P., Bellouin, N., Boucher, O., and Cox, P. M.:  
998 Detection of solar dimming and brightening effects on Northern Hemisphere river flow, *Nat  
999 Geosci*, 7, 796-800, doi:10.1038/ngeo2263, 2014.
- 1000 Gill, A. E.: *Atmosphere-ocean Dynamics*, Academic Press, San Diego, California, USA,  
1001 1982.
- 1002 Gilmanov, T. G., Soussana, J. F., Aires, L., Allard, V., Ammann, C., Balzarolo, M., Barcza,  
1003 Z., Bernhofer, C., Campbell, C. L., Cernusca, A., Cescatti, A., Clifton-Brown, J., Dirks, B. O.  
1004 M., Dore, S., Eugster, W., Fuhrer, J., Gimeno, C., Gruenwald, T., Haszpra, L., Hensen, A.,  
1005 Ibrom, A., Jacobs, A. F. G., Jones, M. B., Lanigan, G., Laurila, T., Lohila, A., G.Manca,  
1006 Marcolla, B., Nagy, Z., Pilegaard, K., Pinter, K., Pio, C., Raschi, A., Rogiers, N., Sanz, M. J.,  
1007 Stefani, P., Sutton, M., Tuba, Z., Valentini, R., Williams, M. L., and Wohlfahrt, G.:  
1008 Partitioning European grassland net ecosystem CO<sub>2</sub> exchange into gross primary productivity  
1009 and ecosystem respiration using light response function analysis, *Agriculture, Ecosystems &  
1010 Environment*, 121, 93-120, 10.1016/j.agee.2006.12.008, 2007.
- 1011 Gocic, M., and Trajkovic, S.: Analysis of trends in reference evapotranspiration data in a  
1012 humid climate, *Hydrological Sciences Journal*, 59, 165-180, 10.1080/02626667.2013.798659,  
1013 2013.
- 1014 Gold, C. M.: Surface interpolation, spatial adjacency and GIS, in: *Three Dimensional  
1015 Applications in Geographical Information Systems*, edited by: Raper, J., Taylor and Francis,  
1016 London, 1989.
- 1017 Green, D. A.: A colour scheme for the display of astronomical intensity images, *Bulletin of  
1018 the Astronomical Society of India*, 39, 2011.
- 1019 Haddeland, I., Clark, D. B., Franssen, W., Ludwig, F., Voß, F., Arnell, N. W., Bertrand, N.,  
1020 Best, M., Folwell, S., Gerten, D., Gomes, S., Gosling, S. N., Hagemann, S., Hanasaki, N.,  
1021 Harding, R., Heinke, J., Kabat, P., Koirala, S., Oki, T., Polcher, J., Stacke, T., Viterbo, P.,  
1022 Weedon, G. P., and Yeh, P.: Multimodel Estimate of the Global Terrestrial Water Balance:  
1023 Setup and First Results, *Journal of Hydrometeorology*, 12, 869-884, 10.1175/2011jhm1324.1,  
1024 2011.
- 1025 Hannaford, J., and Buys, G.: Trends in seasonal river flow regimes in the UK, *Journal of  
1026 Hydrology*, 475, 158-174, doi:10.1016/j.jhydrol.2012.09.044, 2012.
- 1027 Hannaford, J.: Climate-driven changes in UK river flows: A review of the evidence, *Progress  
1028 in Physical Geography*, 39, 29-48, doi:10.1177/0309133314536755, 2015.

- 1029 Harris, I., Jones, P. D., Osborn, T. J., and Lister, D. H.: Updated high-resolution grids of  
 1030 monthly climatic observations - the CRU TS3.10 Dataset, *International Journal of*  
 1031 *Climatology*, 34, 623-642, Doi 10.1002/Joc.3711, 2014.
- 1032 Hartmann, D. L., Klein Tank, A. M. G., Rusticucci, M., Alexander, L. V., Brönnimann, S.,  
 1033 Charabi, Y., Dentener, F. J., Dlugokencky, E. J., Easterling, D. R., Kaplan, A., Soden, B. J.,  
 1034 Thorne, P. W., Wild, M., and Zhai, P. M.: Observations: Atmosphere and Surface, in: *Climate*  
 1035 *Change 2013: The Physical Science Basis. Contribution of Working Group I to the Fifth*  
 1036 *Assessment Report of the Intergovernmental Panel on Climate Change*, edited by: Stocker, T.  
 1037 F., Qin, D., Plattner, G.-K., Tignor, M., Allen, S. K., Boschung, J., Nauels, A., Xia, Y., Bex,  
 1038 V., and Midgley, P. M., Cambridge University Press, Cambridge, United Kingdom and New  
 1039 York, NY, USA, 159–254, 2013.
- 1040 Haslinger, K., and Bartsch, A.: Creating long-term gridded fields of reference  
 1041 evapotranspiration in Alpine terrain based on a recalibrated Hargreaves method, *Hydrology*  
 1042 *and Earth System Sciences*, 20, 1211-1223, 10.5194/hess-20-1211-2016, 2016.
- 1043 Heinemeyer, A., Wilkinson, M., Vargas, R., Subke, J. A., Casella, E., Morison, J. I. L., and  
 1044 Ineson, P.: Exploring the "overflow tap" theory: linking forest soil CO<sub>2</sub> fluxes  
 1045 and individual mycorrhizosphere components to photosynthesis, *Biogeosciences*, 9, 79-95,  
 1046 10.5194/bg-9-79-2012, 2012.
- 1047 Held, I. M., and Soden, B. J.: Robust Responses of the Hydrological Cycle to Global  
 1048 Warming, *Journal of Climate*, 19, 5686-5699, 10.1175/jcli3990.1, 2006.
- 1049 Helmes, L., and Jaenicke, R.: Atmospheric turbidity determined from sunshine records,  
 1050 *Journal of Aerosol Science*, 17, 261-263, doi:10.1016/0021-8502(86)90080-7, 1986.
- 1051 Hickling, R., Roy, D. B., Hill, J. K., Fox, R., and Thomas, C. D.: The distributions of a wide  
 1052 range of taxonomic groups are expanding polewards, *Global Change Biology*, 12, 450-455,  
 1053 doi:10.1111/j.1365-2486.2006.01116.x, 2006.
- 1054 Horn, B. K. P.: Hill Shading and the Reflectance Map, *Proceedings of the Ieee*, 69, 14-47,  
 1055 doi:10.1109/Proc.1981.11918, 1981.
- 1056 Hosseinzadeh Talae, P., Shifteh Some'e, B., and Sobhan Ardakani, S.: Time trend and  
 1057 change point of reference evapotranspiration over Iran, *Theoretical and Applied Climatology*,  
 1058 116, 639-647, 10.1007/s00704-013-0978-x, 2013.
- 1059 Hough, M. N., and Jones, R. J. A.: The United Kingdom Meteorological Office rainfall and  
 1060 evaporation calculation system: MORECS version 2.0-an overview, *Hydrology and Earth*  
 1061 *System Sciences*, 1, 227-239, doi:10.5194/hess-1-227-1997, 1997.
- 1062 IPCC: *Climate Change 2013: The Physical Science Basis. Contribution of Working Group I*  
 1063 *to the Fifth Assessment Report of the Intergovernmental Panel on Climate Change*,  
 1064 Cambridge University Press, Cambridge, United Kingdom and New York, NY, USA, 1535  
 1065 pp., 2013.
- 1066 IPCC: *Climate Change 2014: Impacts, Adaptation, and Vulnerability. Part A: Global and*  
 1067 *Sectoral Aspects. Contribution of Working Group II to the Fifth Assessment Report of the*  
 1068 *Intergovernmental Panel on Climate Change* [Field, C.B., V.R. Barros, D.J. Dokken, K.J.  
 1069 Mach, M.D. Mastrandrea, T.E. Bilir, M. Chatterjee, K.L. Ebi, Y.O. Estrada, R.C. Genova, B.  
 1070 Girma, E.S. Kissel, A.N. Levy, S. MacCracken, P.R. Mastrandrea, and L.L. White (eds.)],  
 1071 Cambridge University Press, Cambridge, United Kingdom and New York, NY, USA, 1132  
 1072 pp., 2014a.

- 1073 IPCC: Climate Change 2014: Impacts, Adaptation, and Vulnerability. Part B: Regional  
 1074 Aspects. Contribution of Working Group II to the Fifth Assessment Report of the  
 1075 Intergovernmental Panel on Climate Change [Barros, V.R., C.B. Field, D.J. Dokken, M.D.  
 1076 Mastrandrea, K.J. Mach, T.E. Bilir, M. Chatterjee, K.L. Ebi, Y.O. Estrada, R.C. Genova, B.  
 1077 Girma, E.S. Kissel, A.N. Levy, S. MacCracken, P.R. Mastrandrea, and L.L. White (eds.)],  
 1078 Cambridge University Press, Cambridge, United Kingdom and New York, NY, USA, 688  
 1079 pp., 2014b.
- 1080 Iqbal, M.: An introduction to solar radiation, Academic Press, London, 1983.
- 1081 Ishibashi, M., and Terashima, I.: Effects of continuous leaf wetness on photosynthesis:  
 1082 adverse aspects of rainfall, *Plant, Cell & Environment*, 18, 431-438, 10.1111/j.1365-  
 1083 3040.1995.tb00377.x, 1995.
- 1084 Jenkins, G. J., Perry, M. C., and Prior, M. J.: The climate of the United Kingdom and recent  
 1085 trends, Met Office Hadley Centre, Exeter, UK, 2008.
- 1086 Jhajharia, D., Dinpashoh, Y., Kahya, E., Singh, V. P., and Fakheri-Fard, A.: Trends in  
 1087 reference evapotranspiration in the humid region of northeast India, *Hydrological Processes*,  
 1088 26, 421-435, 10.1002/hyp.8140, 2012.
- 1089 Jones, P. D., Lister, D. H., Osborn, T. J., Harpham, C., Salmon, M., and Morice, C. P.:  
 1090 Hemispheric and large-scale land-surface air temperature variations: An extensive revision  
 1091 and an update to 2010, *Journal of Geophysical Research: Atmospheres*, 117, n/a-n/a,  
 1092 doi:10.1029/2011JD017139, 2012.
- 1093 CRU TS3.21: Climatic Research Unit (CRU) Time-Series (TS) Version 3.21 of High  
 1094 Resolution Gridded Data of Month-by-month Variation in Climate (Jan. 1901- Dec. 2012).  
 1095 2013.
- 1096 Kay, A. L., Bell, V. A., Blyth, E. M., Crooks, S. M., Davies, H. N., and Reynard, N. S.: A  
 1097 hydrological perspective on evaporation: historical trends and future projections in Britain,  
 1098 *Journal of Water and Climate Change*, 4, 193, doi:10.2166/wcc.2013.014, 2013.
- 1099 Kay, A. L., Rudd, A. C., Davies, H. N., Kendon, E. J., and Jones, R. G.: Use of very high  
 1100 resolution climate model data for hydrological modelling: baseline performance and future  
 1101 flood changes, *Climatic Change*, doi:10.1007/s10584-015-1455-6, 2015.
- 1102 Keller, V. D. J., Tanguy, M., Prosdocimi, I., Terry, J. A., Hitt, O., Cole, S. J., Fry, M., Morris,  
 1103 D. G., and Dixon, H.: CEH-GEAR: 1 km resolution daily and monthly areal rainfall estimates  
 1104 for the UK for hydrological and other applications, *Earth Syst. Sci. Data*, 7, 143-155,  
 1105 doi:10.5194/essd-7-143-2015, 2015.
- 1106 Kimball, B. A., Idso, S. B., and Aase, J. K.: A Model of Thermal-Radiation from Partly  
 1107 Cloudy and Overcast Skies, *Water Resources Research*, 18, 931-936,  
 1108 doi:10.1029/Wr018i004p00931, 1982.
- 1109 Kruijt, B., Witte, J.-P. M., Jacobs, C. M. J., and Kroon, T.: Effects of rising atmospheric CO<sub>2</sub>  
 1110 on evapotranspiration and soil moisture: A practical approach for the Netherlands, *Journal of*  
 1111 *Hydrology*, 349, 257-267, doi:10.1016/j.jhydrol.2007.10.052, 2008.
- 1112 Kume, T., Kuraji, K., Yoshifuji, N., Morooka, T., Sawano, S., Chong, L., and Suzuki, M.:  
 1113 Estimation of canopy drying time after rainfall using sap flow measurements in an emergent  
 1114 tree in a lowland mixed-dipterocarp forest in Sarawak, Malaysia, *Hydrological Processes*, 20,  
 1115 565-578, 10.1002/hyp.5924, 2006.

- 1116 Li, B., Chen, F., and Guo, H.: Regional complexity in trends of potential evapotranspiration  
1117 and its driving factors in the Upper Mekong River Basin, *Quaternary International*, 380-381,  
1118 83-94, 10.1016/j.quaint.2014.12.052, 2015.
- 1119 Li, Y., and Zhou, M.: Trends in Dryness Index Based on Potential Evapotranspiration and  
1120 Precipitation over 1961–2099 in Xinjiang, China, *Advances in Meteorology*, 2014, 1-15,  
1121 10.1155/2014/548230, 2014.
- 1122 Liley, J. B.: New Zealand dimming and brightening, *Journal of Geophysical Research*, 114,  
1123 doi:10.1029/2008jd011401, 2009.
- 1124 Lu, X., Bai, H., and Mu, X.: Explaining the evaporation paradox in Jiangxi Province of  
1125 China: Spatial distribution and temporal trends in potential evapotranspiration of Jiangxi  
1126 Province from 1961 to 2013, *International Soil and Water Conservation Research*, 4, 45-51,  
1127 10.1016/j.iswcr.2016.02.004, 2016.
- 1128 Marsh, T., and Dixon, H.: The UK water balance – how much has it changed in a warming  
1129 world?, 01-05, doi:10.7558/bhs.2012.ns32, 2012.
- 1130 Marthews, T. R., Malhi, Y., and Iwata, H.: Calculating downward longwave radiation under  
1131 clear and cloudy conditions over a tropical lowland forest site: an evaluation of model  
1132 schemes for hourly data, *Theoretical and Applied Climatology*, 107, 461-477,  
1133 10.1007/s00704-011-0486-9, 2011.
- 1134 Matsoukas, C., Benas, N., Hatzianastassiou, N., Pavlakis, K. G., Kanakidou, M., and  
1135 Vardavas, I.: Potential evaporation trends over land between 1983–2008: driven by radiative  
1136 fluxes or vapour-pressure deficit?, *Atmospheric Chemistry and Physics*, 11, 7601-7616,  
1137 doi:10.5194/acp-11-7601-2011, 2011.
- 1138 McVicar, T. R., Van Niel, T. G., Li, L. T., Roderick, M. L., Rayner, D. P., Ricciardulli, L.,  
1139 and Donohue, R. J.: Wind speed climatology and trends for Australia, 1975–2006: Capturing  
1140 the stilling phenomenon and comparison with near-surface reanalysis output, *Geophysical  
1141 Research Letters*, 35, n/a-n/a, 10.1029/2008GL035627, 2008.
- 1142 McVicar, T. R., Roderick, M. L., Donohue, R. J., Li, L. T., Van Niel, T. G., Thomas, A.,  
1143 Grieser, J., Jhajharia, D., Himri, Y., Mahowald, N. M., Mescherskaya, A. V., Kruger, A. C.,  
1144 Rehman, S., and Dinpashoh, Y.: Global review and synthesis of trends in observed terrestrial  
1145 near-surface wind speeds: Implications for evaporation, *Journal of Hydrology*, 416, 182-205,  
1146 doi:10.1016/j.jhydrol.2011.10.024, 2012.
- 1147 Monteith, J. L.: Evaporation and environment, in: 19th Symposia of the Society for  
1148 Experimental Biology, University Press, Cambridge, 1965.
- 1149 Monteith, J. L.: Evaporation and surface temperature, *Quarterly Journal of the Royal  
1150 Meteorological Society*, 107, 1-27, 10.1002/qj.49710745102, 1981.
- 1151 Moors, E.: Water Use of Forests in the Netherlands, PhD, Vrije Universiteit, Amsterdam, the  
1152 Netherlands, 2012.
- 1153 Morris, D. G., and Flavin, R. W.: A digital terrain model for hydrology, *Proceedings of the  
1154 4th International Symposium on Spatial Data Handling*, 1, 250-262, 1990.
- 1155 Morton, D., Rowland, C., Wood, C., Meek, L., Marston, C., Smith, G., Wadsworth, R., and  
1156 Simpson, I. C.: Final Report for LCM2007 - the new UK land cover map, NERC/Centre for  
1157 Ecology & Hydrology 11/07 (CEH Project Number: C03259), 2011.

- 1158 Muneer, T., and Munawwar, S.: Potential for improvement in estimation of solar diffuse  
1159 irradiance, *Energy Conversion and Management*, 47, 68-86,  
1160 doi:10.1016/j.enconman.2005.03.015, 2006.
- 1161 Murphy, J. M., Sexton, D. M. H., Jenkins, G. J., Boorman, P. M., Booth, B. B. B., Brown, C.  
1162 C., Clark, R. T., Collins, M., Harris, G. R., Kendon, E. J., Betts, R. A., Brown, S. J., Howard,  
1163 T. P., Humphrey, K. A., McCarthy, M. P., McDonald, R. E., Stephens, A., Wallace, C.,  
1164 Warren, R., Wilby, R., and Wood, R. A.: UK Climate Projections Science Report: Climate  
1165 change projections, Met Office Hadley Centre, Exeter, 2009.
- 1166 Newton, K., and Burch, S. F.: Estimation of the UK wind energy resource using computer  
1167 modelling techniques and map data, *Energy Technology Support Unit*, 50, 1985.
- 1168 Norton, L. R., Maskell, L. C., Smart, S. S., Dunbar, M. J., Emmett, B. A., Carey, P. D.,  
1169 Williams, P., Crowe, A., Chandler, K., Scott, W. A., and Wood, C. M.: Measuring stock and  
1170 change in the GB countryside for policy--key findings and developments from the  
1171 Countryside Survey 2007 field survey, *Journal of environmental management*, 113, 117-127,  
1172 doi:10.1016/j.jenvman.2012.07.030, 2012.
- 1173 Oldekop, E.: Evaporation from the surface of river basins, in: *Collection of the Works of*  
1174 *Students of the Meteorological Observatory, University of Tartu-Jurjew-Dorpat, Tartu,*  
1175 *Estonia*, 209, 1911.
- 1176 Palmer, W. C.: *Meteorological Drought. Res. Paper No.45, Dept. of Commerce, Washington,*  
1177 *D.C.*, 1965.
- 1178 Paltineanu, C., Chitu, E., and Mateescu, E.: New trends for reference evapotranspiration and  
1179 climatic water deficit, *International Agrophysics*, 26, 10.2478/v10247-012-0023-9, 2012.
- 1180 Parker, D., and Horton, B.: Uncertainties in central England temperature 1878-2003 and some  
1181 improvements to the maximum and minimum series, *International Journal of Climatology*, 25,  
1182 1173-1188, doi:10.1002/joc.1190, 2005.
- 1183 Penman, H. L.: Natural Evaporation from Open Water, Bare Soil and Grass, *Proceedings of*  
1184 *the Royal Society of London. Series A. Mathematical and Physical Sciences*, 193, 120-145,  
1185 10.1098/rspa.1948.0037, 1948.
- 1186 Pocock, M. J., Roy, H. E., Preston, C. D., and Roy, D. B.: The Biological Records Centre in  
1187 the United Kingdom: a pioneer of citizen science., *Biological Journal of the Linnean Society*,  
1188 doi:10.1111/bij.12548, 2015.
- 1189 Prata, A. J.: A new long-wave formula for estimating downward clear-sky radiation at the  
1190 surface, *Quarterly Journal of the Royal Meteorological Society*, 122, 1127-1151,  
1191 doi:10.1002/qj.49712253306, 1996.
- 1192 Prescott, J. A.: Evaporation from a water surface in relation to solar radiation, *Transaction of*  
1193 *the Royal Society of South Australia*, 64, 114-125, 1940.
- 1194 Prudhomme, C., Giuntoli, I., Robinson, E. L., Clark, D. B., Arnell, N. W., Dankers, R.,  
1195 Fekete, B. M., Franssen, W., Gerten, D., Gosling, S. N., Hagemann, S., Hannah, D. M., Kim,  
1196 H., Masaki, Y., Satoh, Y., Stacke, T., Wada, Y., and Wisser, D.: Hydrological droughts in the  
1197 21st century, hotspots and uncertainties from a global multimodel ensemble experiment,  
1198 *Proceedings of the National Academy of Sciences*, 111, 3262-3267,  
1199 doi:10.1073/pnas.1222473110, 2014.

- 1200 Pryor, S. C., Barthelmie, R. J., Young, D. T., Takle, E. S., Arritt, R. W., Flory, D., Gutowski,  
1201 W. J., Nunes, A., and Roads, J.: Wind speed trends over the contiguous United States, *Journal*  
1202 *of Geophysical Research: Atmospheres*, 114, n/a-n/a, 10.1029/2008JD011416, 2009.
- 1203 Reynolds, B., Chamberlain, P. M., Poskitt, J., Woods, C., Scott, W. A., Rowe, E. C.,  
1204 Robinson, D. A., Frogbrook, Z. L., Keith, A. M., Henrys, P. A., Black, H. I. J., and Emmett,  
1205 B. A.: Countryside Survey: National “Soil Change” 1978–2007 for Topsoils in Great  
1206 Britain—Acidity, Carbon, and Total Nitrogen Status, *Vadose Zone Journal*, 12, 0,  
1207 doi:10.2136/vzj2012.0114, 2013.
- 1208 Richards, J. M.: A simple expression for the saturation vapour pressure of water in the range  
1209 –50 to 140°C, *Journal of Physics D: Applied Physics*, 4, L15, 1971.
- 1210 Robinson, E. L., Blyth, E., Clark, D. B., Finch, J., and Rudd, A. C.: Climate hydrology and  
1211 ecology research support system potential evapotranspiration dataset for Great Britain (1961-  
1212 2012) [CHESS-PE], NERC Environmental Information Data Centre, doi:10.5285/d329f4d6-  
1213 95ba-4134-b77a-a377e0755653, 2015a.
- 1214 Robinson, E. L., Blyth, E., Clark, D. B., Finch, J., and Rudd, A. C.: Climate hydrology and  
1215 ecology research support system meteorology dataset for Great Britain (1961-2012) [CHESS-  
1216 met], NERC Environmental Information Data Centre, doi:10.5285/80887755-1426-4dab-  
1217 a4a6-250919d5020c, 2015b.
- 1218 Rodda, J. C., and Marsh, T. J.: The 1975-76 Drought - a contemporary and retrospective  
1219 review, Wallingford, UK, 2011.
- 1220 Roderick, M. L., Rotstayn, L. D., Farquhar, G. D., and Hobbins, M. T.: On the attribution of  
1221 changing pan evaporation, *Geophysical Research Letters*, 34, 10.1029/2007gl031166, 2007.
- 1222 Rotstayn, L. D., Roderick, M. L., and Farquhar, G. D.: A simple pan-evaporation model for  
1223 analysis of climate simulations: Evaluation over Australia, *Geophysical Research Letters*, 33,  
1224 10.1029/2006gl027114, 2006.
- 1225 Rudd, A. C., and Kay, A. L.: Use of very high resolution climate model data for hydrological  
1226 modelling: estimation of potential evaporation, *Hydrology Research*,  
1227 doi:10.2166/nh.2015.028, 2015.
- 1228 Rutter, A. J., Kershaw, K. A., Robins, P. C., and Morton, A. J.: A predictive model of rainfall  
1229 interception in forests, 1. Derivation of the model from observations in a plantation of  
1230 Corsican pine, *Agricultural Meteorology*, 9, 367-384, doi:10.1016/0002-1571(71)90034-3,  
1231 1971.
- 1232 Sanchez-Lorenzo, A., Calbó, J., and Martin-Vide, J.: Spatial and Temporal Trends in  
1233 Sunshine Duration over Western Europe (1938–2004), *Journal of Climate*, 21, 6089-6098,  
1234 doi:10.1175/2008jcli2442.1, 2008.
- 1235 Sanchez-Lorenzo, A., Calbó, J., Brunetti, M., and Deser, C.: Dimming/brightening over the  
1236 Iberian Peninsula: Trends in sunshine duration and cloud cover and their relations with  
1237 atmospheric circulation, *Journal of Geophysical Research*, 114, doi:10.1029/2008jd011394,  
1238 2009.
- 1239 Sanchez-Lorenzo, A., and Wild, M.: Decadal variations in estimated surface solar radiation  
1240 over Switzerland since the late 19th century, *Atmospheric Chemistry and Physics*, 12, 8635-  
1241 8644, doi:10.5194/acp-12-8635-2012, 2012.
- 1242 Sanchez-Romero, A., Sanchez-Lorenzo, A., Calbó, J., González, J. A., and Azorin-Molina,  
1243 C.: The signal of aerosol-induced changes in sunshine duration records: A review of the

- 1244 evidence, *Journal of Geophysical Research: Atmospheres*, 119, 4657-4673,  
1245 doi:10.1002/2013JD021393, 2014.
- 1246 Scheff, J., and Frierson, D. M. W.: Scaling Potential Evapotranspiration with Greenhouse  
1247 Warming, *Journal of Climate*, 27, 1539-1558, doi:10.1175/JCLI-D-13-00233.1, 2014.
- 1248 Schneider, T., O'Gorman, P. A., and Levine, X. J.: Water Vapor and the Dynamics of Climate  
1249 Changes, *Reviews of Geophysics*, 48, 10.1029/2009rg000302, 2010.
- 1250 Schymanski, S. J., and Or, D.: Wind effects on leaf transpiration challenge the concept of  
1251 "potential evaporation", *Proceedings of the International Association of Hydrological  
1252 Sciences*, 371, 99-107, 10.5194/piahs-371-99-2015, 2015.
- 1253 Shan, N., Shi, Z., Yang, X., Zhang, X., Guo, H., Zhang, B., and Zhang, Z.: Trends in potential  
1254 evapotranspiration from 1960 to 2013 for a desertification-prone region of China,  
1255 *International Journal of Climatology*, n/a-n/a, 10.1002/joc.4566, 2015.
- 1256 Sheffield, J., Goteti, G., and Wood, E. F.: Development of a 50-Year High-Resolution Global  
1257 Dataset of Meteorological Forcings for Land Surface Modeling, *Journal of Climate*, 19, 3088-  
1258 3111, doi:10.1175/JCLI3790.1, 2006.
- 1259 Shuttleworth, W. J.: *Terrestrial Hydrometeorology*, John Wiley & Sons, Ltd, 2012.
- 1260 Song, Z. W. Z., H. L. ; Snyder, R. L. ; Anderson, F. E. ; Chen, F. : Distribution and Trends in  
1261 Reference Evapotranspiration in the North China Plain, *Journal of Irrigation and Drainage  
1262 Engineering*, 136, 240-247, doi:10.1061/(ASCE)IR.1943-4774.0000175, 2010.
- 1263 Soussana, J. F., Allard, V., Pilegaard, K., Ambus, P., Amman, C., Campbell, C., Ceschia, E.,  
1264 Clifton-Brown, J., Czobel, S., Domingues, R., Flechard, C., Fuhrer, J., Hensen, A., Horvath,  
1265 L., Jones, M., Kasper, G., Martin, C., Nagy, Z., Neftel, A., Raschi, A., Baronti, S., Rees, R.  
1266 M., Skiba, U., Stefani, P., Manca, G., Sutton, M., Tuba, Z., and Valentini, R.: Full accounting  
1267 of the greenhouse gas (CO<sub>2</sub>, N<sub>2</sub>O, CH<sub>4</sub>) budget of nine European grassland sites,  
1268 *Agriculture, Ecosystems & Environment*, 121, 121-134, 10.1016/j.agee.2006.12.022, 2007.
- 1269 Stanhill, G., and Cohen, S.: Solar Radiation Changes in the United States during the  
1270 Twentieth Century: Evidence from Sunshine Duration Measurements, *Journal of Climate*, 18,  
1271 1503-1512, doi:10.1175/JCLI3354.1, 2005.
- 1272 Stanhill, G., and Möller, M.: Evaporative climate change in the British Isles, *International  
1273 Journal of Climatology*, 28, 1127-1137, doi:10.1002/joc.1619, 2008.
- 1274 Stewart, J. B.: On the use of the Penman-Monteith equation for determining areal  
1275 evapotranspiration, in: *Estimation of Areal Evapotranspiration (Proceedings of a workshop  
1276 held at Vancouver, B.C., Canada, August 1987)*. edited by: Black, T. A. S., D. L.; Novak, M.  
1277 D.; Price, D. T., IAHS, Wallingford, Oxfordshire, UK, 1989.
- 1278 Sutton, R. T., and Dong, B.: Atlantic Ocean influence on a shift in European climate in the  
1279 1990s, *Nature Geosci*, 5, 788-792, doi:10.1038/ngeo1595, 2012.
- 1280 Tabari, H., Nikbakht, J., and Hosseinzadeh Talaei, P.: Identification of Trend in Reference  
1281 Evapotranspiration Series with Serial Dependence in Iran, *Water Resources Management*, 26,  
1282 2219-2232, 10.1007/s11269-012-0011-7, 2012.
- 1283 Tanguy, M., Dixon, H., Prosdocimi, I., Morris, D. G., and Keller, V. D. J.: Gridded estimates  
1284 of daily and monthly areal rainfall for the United Kingdom (1890-2012) [CEH-GEAR],  
1285 NERC Environmental Information Data Centre, doi:10.5285/5dc179dc-f692-49ba-9326-  
1286 a6893a503f6e, 2014.



1287 Thackeray, S. J., Sparks, T. H., Frederiksen, M., Burthe, S., Bacon, P. J., Bell, J. R., Botham,  
1288 M. S., Brereton, T. M., Bright, P. W., Carvalho, L., Clutton-Brock, T., Dawson, A., Edwards,  
1289 M., Elliott, J. M., Harrington, R., Johns, D., Jones, I. D., Jones, J. T., Leech, D. I., Roy, D. B.,  
1290 Scott, W. A., Smith, M., Smithers, R. J., Winfield, I. J., and Wanless, S.: Trophic level  
1291 asynchrony in rates of phenological change for marine, freshwater and terrestrial  
1292 environments, *Global Change Biology*, 16, 3304-3313, doi:10.1111/j.1365-  
1293 2486.2010.02165.x, 2010.

1294 Thompson, N., Barrie, I. A., and Ayles, M.: The Meteorological Office rainfall and  
1295 evaporation calculation system: MORECS, Meteorological Office, Bracknell, 1981.

1296 Vautard, R., Cattiaux, J., Yiou, P., Thepaut, J. N., and Ciais, P.: Northern Hemisphere  
1297 atmospheric stilling partly attributed to an increase in surface roughness, *Nat Geosci*, 3, 756-  
1298 761, doi:10.1038/Ngeo979, 2010.

1299 Vicente-Serrano, S. M., Azorin-Molina, C., Sanchez-Lorenzo, A., Revuelto, J., López-  
1300 Moreno, J. I., González-Hidalgo, J. C., Moran-Tejeda, E., and Espejo, F.: Reference  
1301 evapotranspiration variability and trends in Spain, 1961–2011, *Global and Planetary Change*,  
1302 121, 26-40, 10.1016/j.gloplacha.2014.06.005, 2014.

1303 Vicente-Serrano, S. M., Azorin-Molina, C., Sanchez-Lorenzo, A., El Kenawy, A., Martín-  
1304 Hernández, N., Peña-Gallardo, M., Beguería, S., and Tomas-Burguera, M.: Recent changes  
1305 and drivers of the atmospheric evaporative demand in the Canary Islands, *Hydrology and*  
1306 *Earth System Sciences*, 20, 3393-3410, 10.5194/hess-20-3393-2016, 2016.

1307 Vincent, L. A., Zhang, X., Brown, R. D., Feng, Y., Mekis, E., Milewska, E. J., Wan, H., and  
1308 Wang, X. L.: Observed Trends in Canada's Climate and Influence of Low-Frequency  
1309 Variability Modes, *Journal of Climate*, 28, 4545-4560, 10.1175/jcli-d-14-00697.1, 2015.

1310 von Storch, H., and Zwiers, F. W.: *Statistical analysis in climate research*, Cambridge  
1311 University Press, Cambridge ; New York, x, 484 p. pp., 1999.

1312 Wang, K., and Liang, S.: Global atmospheric downward longwave radiation over land surface  
1313 under all-sky conditions from 1973 to 2008, *Journal of Geophysical Research*, 114,  
1314 doi:10.1029/2009jd011800, 2009.

1315 Ward, R. C., and Robinson, M.: *Principles of Hydrology*, McGraw Hill, 2000.

1316 Watts, G., Battarbee, R. W., Bloomfield, J. P., Crossman, J., Daccache, A., Durance, I.,  
1317 Elliott, J. A., Garner, G., Hannaford, J., Hannah, D. M., Hess, T., Jackson, C. R., Kay, A. L.,  
1318 Kernan, M., Knox, J., Mackay, J., Monteith, D. T., Ormerod, S. J., Rance, J., Stuart, M. E.,  
1319 Wade, A. J., Wade, S. D., Weatherhead, K., Whitehead, P. G., and Wilby, R. L.: Climate  
1320 change and water in the UK - past changes and future prospects, *Progress in Physical*  
1321 *Geography*, 39, 6-28, doi:10.1177/0309133314542957, 2015.

1322 Weedon, G. P., Gomes, S., Viterbo, P., Shuttleworth, W. J., Blyth, E., Osterle, H., Adam, J.  
1323 C., Bellouin, N., Boucher, O., and Best, M.: Creation of the WATCH Forcing Data and Its  
1324 Use to Assess Global and Regional Reference Crop Evaporation over Land during the  
1325 Twentieth Century, *J Hydrometeorol*, 12, 823-848, doi:10.1175/2011jhm1369.1, 2011.

1326 Weedon, G. P., Balsamo, G., Bellouin, N., Gomes, S., Best, M. J., and Viterbo, P.: The  
1327 WFDEI meteorological forcing data set: WATCH Forcing Data methodology applied to  
1328 ERA-Interim reanalysis data, *Water Resources Research*, 50, 7505-7514,  
1329 doi:10.1002/2014WR015638, 2014.

1330 Wild, M.: Global dimming and brightening: A review, *Journal of Geophysical Research*, 114,  
1331 doi:10.1029/2008jd011470, 2009.

1332 Wilkinson, M., Eaton, E. L., Broadmeadow, M. S. J., and Morison, J. I. L.: Inter-annual  
1333 variation of carbon uptake by a plantation oak woodland in south-eastern England,  
1334 *Biogeosciences*, 9, 5373-5389, 10.5194/bg-9-5373-2012, 2012.

1335 Willett, K. M., Dunn, R. J. H., Thorne, P. W., Bell, S., de Podesta, M., Parker, D. E., Jones, P.  
1336 D., and Williams Jr, C. N.: HadISDH land surface multi-variable humidity and temperature  
1337 record for climate monitoring, *Climate of the Past*, 10, 1983-2006, 10.5194/cp-10-1983-2014,  
1338 2014.

1339 WMO: Manual on the Global Observing System, Secretariat of the World Meteorological  
1340 Organization, Geneva, Switzerland, 2013.

1341 Wood, C. M., Smart, S. M., and Bunce, R. G. H.: Woodland survey of Great Britain 1971–  
1342 2001, *Earth System Science Data Discussions*, 8, 259-277, doi:10.5194/essdd-8-259-2015,  
1343 2015.

1344 Yin, Y., Wu, S., Chen, G., and Dai, E.: Attribution analyses of potential evapotranspiration  
1345 changes in China since the 1960s, *Theoretical and Applied Climatology*, 101, 19-28,  
1346 10.1007/s00704-009-0197-7, 2009.

1347 Zhang, K.-x., Pan, S.-m., Zhang, W., Xu, Y.-h., Cao, L.-g., Hao, Y.-p., and Wang, Y.:  
1348 Influence of climate change on reference evapotranspiration and aridity index and their  
1349 temporal-spatial variations in the Yellow River Basin, China, from 1961 to 2012, *Quaternary  
1350 International*, 380-381, 75-82, 10.1016/j.quaint.2014.12.037, 2015.

1351 Zhao, J., Xu, Z.-x., Zuo, D.-p., and Wang, X.-m.: Temporal variations of reference  
1352 evapotranspiration and its sensitivity to meteorological factors in Heihe River Basin, China,  
1353 *Water Science and Engineering*, 8, 1-8, 10.1016/j.wse.2015.01.004, 2015.

1354 Zwiers, F. W., and von Storch, H.: Taking Serial-Correlation into Account in Tests of the  
1355 Mean, *Journal of Climate*, 8, 336-351, doi:10.1175/1520-  
1356 0442(1995)008<0336:Tsciai>2.0.Co;2, 1995.

1357

1358

1359 Table 1. Description of input meteorological variables

Variable (units)	Source data	Ancillary files	Assumptions	Height
Air temperature (K)	MORECS air temperature	IHDTM elevation	Lapsed to IHDTM elevation	1.2 m
Specific humidity (kg kg <sup>-1</sup> )	MORECS vapour pressure	IHDTM elevation	Lapsed to IHDTM elevation  Constant air pressure = 100 kPa	1.2 m
Downward LW radiation (W m <sup>-2</sup> )	MORECS air temperature, vapour pressure, sunshine hours	IHDTM elevation	Constant cloud base height	1.2 m
Downward SW radiation (W m <sup>-2</sup> )	MORECS sunshine hours	IHDTM elevation  Spatially-varying aerosol correction	No time-varying aerosol correction	1.2 m
Wind speed (m s <sup>-1</sup> )	MORECS wind speed	ETSU average wind speeds	Wind speed correction is constant	10 m
Precipitation (kg m <sup>-2</sup> s <sup>-1</sup> )	CEH-GEAR precipitation	-	No transformations performed	n/a
Daily temperature range (K)	CRU TS 3.21 daily temperature range	-	No spatial interpolation from 0.5° resolution.  No temporal interpolation	1.2 m

---

			(constant values for each month)	
Surface air pressure (Pa)	WFD air pressure	IHD TM elevation	Mean-monthly values from WFD used (each year has same values). Lapsed to IHD TM elevation. No temporal interpolation (constant values for each month).	n/a

---

1360  
1361

1362 Table 2: Rate of change of annual means of meteorological and potential evapotranspiration  
 1363 variables in Great Britain. Bold indicates trends that are significant at the 5% level. The  
 1364 ranges are given by the 95% CI.

Variable	Rate of change $\pm$ 95% CI				
	Great Britain	England	Scotland	Wales	English lowlands
Air temperature (K dec <sup>-1</sup> )	<b>0.21 <math>\pm</math> 0.15</b>	<b>0.23 <math>\pm</math> 0.14</b>	<b>0.17 <math>\pm</math> 0.12</b>	<b>0.21 <math>\pm</math> 0.15</b>	<b>0.25 <math>\pm</math> 0.17</b>
Specific humidity (g kg <sup>-1</sup> dec <sup>-1</sup> )	<b>0.049 <math>\pm</math> 0.037</b>	<b>0.054 <math>\pm</math> 0.04</b>	<b>0.040 <math>\pm</math> 0.036</b>	<b>0.055 <math>\pm</math> 0.037</b>	<b>0.053 <math>\pm</math> 0.044</b>
Downward SW radiation (W m <sup>-2</sup> dec <sup>-1</sup> )	<b>1.0 <math>\pm</math> 0.8</b>	<b>1.3 <math>\pm</math> 1.0</b>	0.5 $\pm$ 0.6	<b>1.1 <math>\pm</math> 0.9</b>	<b>1.5 <math>\pm</math> 1.0</b>
Downward LW radiation (W m <sup>-2</sup> dec <sup>-1</sup> )	<b>0.50 <math>\pm</math> 0.48</b>	0.45 $\pm$ 0.48	<b>0.58 <math>\pm</math> 0.48</b>	0.50 $\pm$ 0.55	0.42 $\pm$ 0.48
Wind speed (m s <sup>-1</sup> dec <sup>-1</sup> )	<b>-0.18 <math>\pm</math> 0.09</b>	<b>-0.16 <math>\pm</math> 0.09</b>	<b>-0.20 <math>\pm</math> 0.10</b>	<b>-0.25 <math>\pm</math> 0.16</b>	<b>-0.13 <math>\pm</math> 0.07</b>
Precipitation (mm d <sup>-1</sup> dec <sup>-1</sup> )	<b>0.08 <math>\pm</math> 0.06</b>	0.04 $\pm$ 0.06	<b>0.14 <math>\pm</math> 0.09</b>	0.08 $\pm$ 0.09	0.03 $\pm$ 0.05
Daily temperature range (K dec <sup>-1</sup> )	-0.06 $\pm$ 0.06	-0.03 $\pm$ 0.06	<b>-0.13 <math>\pm</math> 0.08</b>	0.00 $\pm$ 0.06	-0.04 $\pm$ 0.07
Relative humidity (% dec <sup>-1</sup> )	-0.39 $\pm$ 0.44	-0.43 $\pm$ 0.46	-0.33 $\pm$ 0.33	-0.36 $\pm$ 0.4	-0.50 $\pm$ 0.53
PET (mm d <sup>-1</sup> dec <sup>-1</sup> )	<b>0.021 <math>\pm</math> 0.021</b>	<b>0.025 <math>\pm</math> 0.024</b>	<b>0.015 <math>\pm</math> 0.015</b>	0.017 $\pm$ 0.021	<b>0.03 <math>\pm</math> 0.026</b>
Radiative component of PET (mm d <sup>-1</sup> dec <sup>-1</sup> )	<b>0.016 <math>\pm</math> 0.010</b>	<b>0.018 <math>\pm</math> 0.011</b>	<b>0.013 <math>\pm</math> 0.008</b>	<b>0.020 <math>\pm</math> 0.013</b>	<b>0.018 <math>\pm</math> 0.011</b>
Aerodynamic component of PET (mm d <sup>-1</sup> dec <sup>-1</sup> )	0.007 $\pm$ 0.011	0.009 $\pm$ 0.013	0.004 $\pm$ 0.009	0.001 $\pm$ 0.013	0.015 $\pm$ 0.015
PETI (mm d <sup>-1</sup> dec <sup>-1</sup> )	0.019 $\pm$ 0.020	<b>0.023 <math>\pm</math> 0.023</b>	0.014 $\pm$ 0.014	0.016 $\pm$ 0.020	<b>0.028 <math>\pm</math> 0.025</b>

1365

1366 Table 3. Contributions to the rate of change of PET and its radiative and aerodynamic  
 1367 components. For each variable, the first column shows the contribution calculated using  
 1368 regional averages, along with the associated 95% CI. The second column shows the  
 1369 contribution calculated at 1 km resolution, then averaged over each region. The uncertainty on  
 1370 this value is difficult to calculate as the pixels are highly spatially correlated, so the  
 1371 uncertainty range from the regional analysis is used in Fig. 13.

a) Contribution to rate of change of PET (mm d <sup>-1</sup> decade <sup>-1</sup> )												
	Air temperature		Specific humidity		Wind speed		Downward LW		Downward SW		Total	
	Regional	Pixel	Regional	Pixel	Regional	Pixel	Regional	Pixel	Regional	Pixel	Regional	Pixel
England	<b>0.041</b> ± <b>0.025</b>	0.039	<b>-0.025</b> ± <b>0.019</b>	-0.024	<b>-0.010</b> ± <b>0.005</b>	-0.007	0.005 ± 0.006	0.005	<b>0.013</b> ± <b>0.009</b>	0.012	0.025 ± 0.034	0.024
Scotland	<b>0.029</b> ± <b>0.021</b>	0.023	<b>-0.020</b> ± <b>0.018</b>	-0.017	<b>-0.010</b> ± <b>0.005</b>	-0.007	<b>0.006</b> ± <b>0.005</b>	0.006	0.005 ± 0.005	0.004	0.010 ± 0.029	0.008
Wales	<b>0.039</b> ± <b>0.028</b>	0.036	<b>-0.026</b> ± <b>0.018</b>	-0.025	<b>-0.011</b> ± <b>0.007</b>	-0.009	0.006 ± 0.006	0.006	<b>0.010</b> ± <b>0.009</b>	0.009	0.017 ± 0.036	0.017
English lowlands	<b>0.043</b> ± <b>0.029</b>	0.042	<b>-0.024</b> ± <b>0.020</b>	-0.023	<b>-0.008</b> ± <b>0.004</b>	-0.008	0.005 ± 0.006	0.005	<b>0.015</b> ± <b>0.010</b>	0.015	0.031 ± 0.038	0.030
Great Britain	<b>0.037</b> ± <b>0.026</b>	0.031	<b>-0.023</b> ± <b>0.018</b>	-0.022	<b>-0.010</b> ± <b>0.005</b>	-0.007	<b>0.006</b> ± <b>0.005</b>	0.005	<b>0.010</b> ± <b>0.007</b>	0.007	0.019 ± 0.033	0.014
b) Contribution to rate of change of radiative component of (mm d <sup>-1</sup> decade <sup>-1</sup> )												
	Air temperature		Specific humidity		Wind speed		Downward LW		Downward SW		Total	
	Regional	Pixel	Regional	Pixel	Regional	Pixel	Regional	Pixel	Regional	Pixel	Regional	Pixel
England	<b>-0.009</b> ± <b>0.006</b>	-0.009	n/a	n/a	<b>0.009</b> ± <b>0.005</b>	0.007	0.005 ± 0.006	0.005	<b>0.014</b> ± <b>0.010</b>	0.013	<b>0.018</b> ± <b>0.013</b>	0.016
Scotland	<b>-0.006</b> ± <b>0.005</b>	-0.006	n/a	n/a	<b>0.009</b> ± <b>0.004</b>	0.007	<b>0.006</b> ± <b>0.005</b>	0.006	0.005 ± 0.005	0.004	<b>0.014</b> ± <b>0.010</b>	0.012
Wales	<b>-0.007</b> ± <b>0.005</b>	-0.007	n/a	n/a	<b>0.014</b> ± <b>0.009</b>	0.013	0.006 ± 0.006	0.006	<b>0.010</b> ± <b>0.009</b>	0.010	<b>0.023</b> ± <b>0.015</b>	0.022
English lowlands	<b>-0.010</b> ± <b>0.007</b>	-0.010	n/a	n/a	<b>0.007</b> ± <b>0.004</b>	0.006	0.005 ± 0.006	0.005	<b>0.016</b> ± <b>0.011</b>	0.015	<b>0.017</b> ± <b>0.014</b>	0.017
Great Britain	<b>-0.008</b> ± <b>0.006</b>	-0.007	n/a	n/a	<b>0.009</b> ± <b>0.005</b>	0.007	<b>0.006</b> ± <b>0.006</b>	0.006	<b>0.010</b> ± <b>0.008</b>	0.008	<b>0.017</b> ± <b>0.012</b>	0.013
c) Contribution to rate of change of aerodynamic component of PET (mm d <sup>-1</sup> decade <sup>-1</sup> )												
	Air temperature		Specific humidity		Wind speed		Downward LW		Downward SW		Total	
	Regional	Pixel	Regional	Pixel	Regional	Pixel	Regional	Pixel	Regional	Pixel	Regional	Pixel

England	<b>0.052</b> ± <b>0.032</b>	0.050	<b>-0.026</b> ± <b>0.020</b>	-0.026	<b>-0.018</b> ± <b>0.010</b>	-0.015	n/a	n/a	n/a	n/a	0.007 ± 0.039	0.009
Scotland	<b>0.037</b> ± <b>0.027</b>	0.033	<b>-0.021</b> ± <b>0.019</b>	-0.019	<b>-0.019</b> ± <b>0.010</b>	-0.015	n/a	n/a	n/a	n/a	-0.003 ± 0.034	-0.001
Wales	<b>0.048</b> ± <b>0.035</b>	0.046	<b>-0.028</b> ± <b>0.019</b>	-0.027	<b>-0.026</b> ± <b>0.016</b>	-0.023	n/a	n/a	n/a	n/a	-0.005 ± 0.042	-0.003
England and Wales	<b>0.056</b> ± <b>0.037</b>	0.055	<b>-0.026</b> ± <b>0.021</b>	-0.025	<b>-0.015</b> ± <b>0.008</b>	-0.014	n/a	n/a	n/a	n/a	0.015 ± 0.044	0.015
Great Britain	<b>0.046</b> ± <b>0.033</b>	0.041	<b>-0.025</b> ± <b>0.019</b>	-0.023	<b>-0.020</b> ± <b>0.010</b>	-0.015	n/a	n/a	n/a	n/a	0.002 ± 0.039	0.003

1372  
1373

1374 Table 4. Contribution of the trend in each variable to the trends in annual mean PET and its  
 1375 radiative and aerodynamic components as a percentage of the fitted trend in PET and its  
 1376 components.

a) Potential evapotranspiration (PET)						
	Air temperature	Specific humidity	Wind speed	Downward LW	Downward SW	Total
England	154 %	-88 %	-22 %	17 %	47 %	108 %
Scotland	150 %	-74 %	-23 %	26 %	18 %	97 %
Wales	200 %	-130 %	-38 %	28 %	50 %	109 %
English lowlands	142 %	-77 %	-20 %	15 %	45 %	105 %
Great Britain	155 %	-87 %	-23 %	19 %	31 %	96 %
b) Radiative component of PET						
	Air temperature	Specific humidity	Wind speed	Downward LW	Downward SW	Total
England	-47 %	n/a	40 %	28 %	71 %	92 %
Scotland	-42 %	n/a	62 %	46 %	36 %	102 %
Wales	-34 %	n/a	69 %	29 %	52 %	116 %
English lowlands	-53 %	n/a	35 %	27 %	86 %	95 %
Great Britain	-44 %	n/a	46 %	31 %	53 %	87 %
c) Aerodynamic component of PET						
	Air temperature	Specific humidity	Wind speed	Downward LW	Downward SW	Total
England	245 %	-115 %	-48 %	n/a	n/a	82 %
Scotland	68 %	-14 %	-33 %	n/a	n/a	21 %
Wales	-135 %	72 %	-42 %	n/a	n/a	-105 %
English lowlands	282 %	-126 %	-47 %	n/a	n/a	109 %
Great Britain	168 %	-76 %	-44 %	n/a	n/a	48 %

1377  
 1378



1379 Table 5. Contributions to the rate of change of PET and its radiative and aerodynamic  
 1380 components when relative humidity is used. For each variable, the first column shows the  
 1381 contribution calculated using regional averages, along with the associated 95% CI. The  
 1382 second column shows the contribution calculated at 1 km resolution, then averaged over each  
 1383 region. The uncertainty on this value is difficult to calculate as the pixels are highly spatially  
 1384 correlated, so the uncertainty range from the regional analysis is used in Fig. 13.

a) Contribution to rate of change of PET (mm d <sup>-1</sup> decade <sup>-1</sup> )												
	Air temperature		Relative humidity		Wind speed		Downward LW		Downward SW		Total	
	Regional	Pixel	Regional	Pixel	Regional	Pixel	Regional	Pixel	Regional	Pixel	Regional	Pixel
England	<b>-0.002</b> ± <b>0.001</b>	-0.000	0.015 ± 0.016	0.013	<b>-0.010</b> ± <b>0.005</b>	-0.007	0.005 ± 0.006	0.005	<b>0.013</b> ± <b>0.009</b>	0.012	<b>0.021</b> ± <b>0.020</b>	0.023
Scotland	<b>-0.001</b> ± <b>0.001</b>	0.000	0.011 ± 0.011	0.008	<b>-0.010</b> ± <b>0.005</b>	-0.007	<b>0.006</b> ± <b>0.005</b>	0.006	0.005 ± 0.005	0.004	0.010 ± 0.014	0.011
Wales	<b>-0.002</b> ± <b>0.001</b>	-0.000	0.013 ± 0.014	0.012	<b>-0.011</b> ± <b>0.007</b>	-0.009	0.006 ± 0.006	0.006	<b>0.010</b> ± <b>0.009</b>	0.009	0.015 ± 0.019	0.018
English lowlands	<b>-0.003</b> ± <b>0.002</b>	-0.000	0.017 ± 0.018	0.017	<b>-0.008</b> ± <b>0.004</b>	-0.008	0.005 ± 0.006	0.005	<b>0.015</b> ± <b>0.010</b>	0.015	<b>0.026</b> ± <b>0.022</b>	0.028
Great Britain	<b>-0.002</b> ± <b>0.001</b>	0.000	0.013 ± 0.015	0.011	<b>-0.010</b> ± <b>0.005</b>	-0.007	<b>0.006</b> ± <b>0.005</b>	0.005	<b>0.010</b> ± <b>0.007</b>	0.007	0.016 ± 0.018	0.016
b) Contribution to rate of change of radiative component of (mm d <sup>-1</sup> decade <sup>-1</sup> )												
	Air temperature		Relative humidity		Wind speed		Downward LW		Downward SW		Total	
	Regional	Pixel	Regional	Pixel	Regional	Pixel	Regional	Pixel	Regional	Pixel	Regional	Pixel
England	<b>-0.009</b> ± <b>0.006</b>	-0.009	n/a	n/a	<b>0.009</b> ± <b>0.005</b>	0.007	0.005 ± 0.006	0.005	<b>0.014</b> ± <b>0.010</b>	0.013	<b>0.018</b> ± <b>0.013</b>	0.016
Scotland	<b>-0.006</b> ± <b>0.005</b>	-0.006	n/a	n/a	<b>0.009</b> ± <b>0.004</b>	0.007	<b>0.006</b> ± <b>0.005</b>	0.006	0.005 ± 0.005	0.004	<b>0.014</b> ± <b>0.010</b>	0.012
Wales	<b>-0.007</b> ± <b>0.005</b>	-0.007	n/a	n/a	<b>0.014</b> ± <b>0.009</b>	0.013	0.006 ± 0.006	0.006	<b>0.010</b> ± <b>0.009</b>	0.010	<b>0.023</b> ± <b>0.015</b>	0.022
English lowlands	<b>-0.010</b> ± <b>0.007</b>	-0.010	n/a	n/a	<b>0.007</b> ± <b>0.004</b>	0.006	0.005 ± 0.006	0.005	<b>0.016</b> ± <b>0.011</b>	0.015	<b>0.017</b> ± <b>0.014</b>	0.017
Great Britain	<b>-0.008</b> ± <b>0.006</b>	-0.007	n/a	n/a	<b>0.009</b> ± <b>0.005</b>	0.007	<b>0.006</b> ± <b>0.006</b>	0.006	<b>0.010</b> ± <b>0.008</b>	0.008	<b>0.017</b> ± <b>0.012</b>	0.013
c) Contribution to rate of change of aerodynamic component of PET (mm d <sup>-1</sup> decade <sup>-1</sup> )												
	Air temperature		Relative humidity		Wind speed		Downward LW		Downward SW		Total	
	Regional	Pixel	Regional	Pixel	Regional	Pixel	Regional	Pixel	Regional	Pixel	Regional	Pixel

England	<b>0.006</b> ± <b>0.004</b>	0.006	0.015 ± 0.017	0.014	<b>-0.018</b> ± <b>0.010</b>	-0.015	n/a	n/a	n/a	n/a	0.003 ± 0.020	0.004
Scotland	<b>0.004</b> ± <b>0.003</b>	0.004	0.011 ± 0.011	0.009	<b>-0.019</b> ± <b>0.010</b>	-0.015	n/a	n/a	n/a	n/a	-0.004 ± 0.015	-0.002
Wales	<b>0.005</b> ± <b>0.004</b>	0.005	0.013 ± 0.015	0.012	<b>-0.026</b> ± <b>0.016</b>	-0.023	n/a	n/a	n/a	n/a	-0.007 ± 0.022	-0.006
English lowlands	<b>0.007</b> ± <b>0.004</b>	0.006	0.018 ± 0.019	0.017	<b>-0.015</b> ± <b>0.008</b>	-0.014	n/a	n/a	n/a	n/a	0.009 ± 0.021	0.010
Great Britain	<b>0.005</b> ± <b>0.004</b>	0.005	0.014 ± 0.015	0.011	<b>-0.020</b> ± <b>0.010</b>	-0.015	n/a	n/a	n/a	n/a	-0.001 ± 0.019	0.000

1385  
1386

1387 Table 6. Contribution of the trend in each variable to the trends in annual mean PET and its  
 1388 radiative and aerodynamic components as a percentage of the fitted trend in PET and its  
 1389 components when relative humidity is used.

a) Potential evapotranspiration (PET)						
	Air temperature	Relative humidity	Wind speed	Downward LW	Downward SW	Total
England	-0%	57%	-22%	17%	47%	99%
Scotland	0%	65%	-23%	26%	18%	85%
Wales	-0%	68%	-38%	27%	50%	107%
English lowlands	-0%	57%	-20%	15%	45%	97%
Great Britain	0%	60%	-23%	19%	31%	87%
b) Radiative component of PET						
	Air temperature	Relative humidity	Wind speed	Downward LW	Downward SW	Total
England	-47%	n/a	40%	28%	71%	92%
Scotland	-42%	n/a	62%	46%	36%	102%
Wales	-34%	n/a	69%	29%	52%	116%
English lowlands	-53%	n/a	35%	27%	86%	95%
Great Britain	-44%	n/a	46%	31%	53%	87%
c) Aerodynamic component of PET						
	Air temperature	Relative humidity	Wind speed	Downward LW	Downward SW	Total
England	29%	78%	-48%	n/a	n/a	59%
Scotland	8%	14%	-33%	n/a	n/a	-11%
Wales	-15%	-33%	-42%	n/a	n/a	-90%
English lowlands	33%	98%	-47%	n/a	n/a	84%
Great Britain	19%	52%	-44%	n/a	n/a	27%

1390  
 1391

1392 Table A1. Details of sites used for validation of meteorological data.

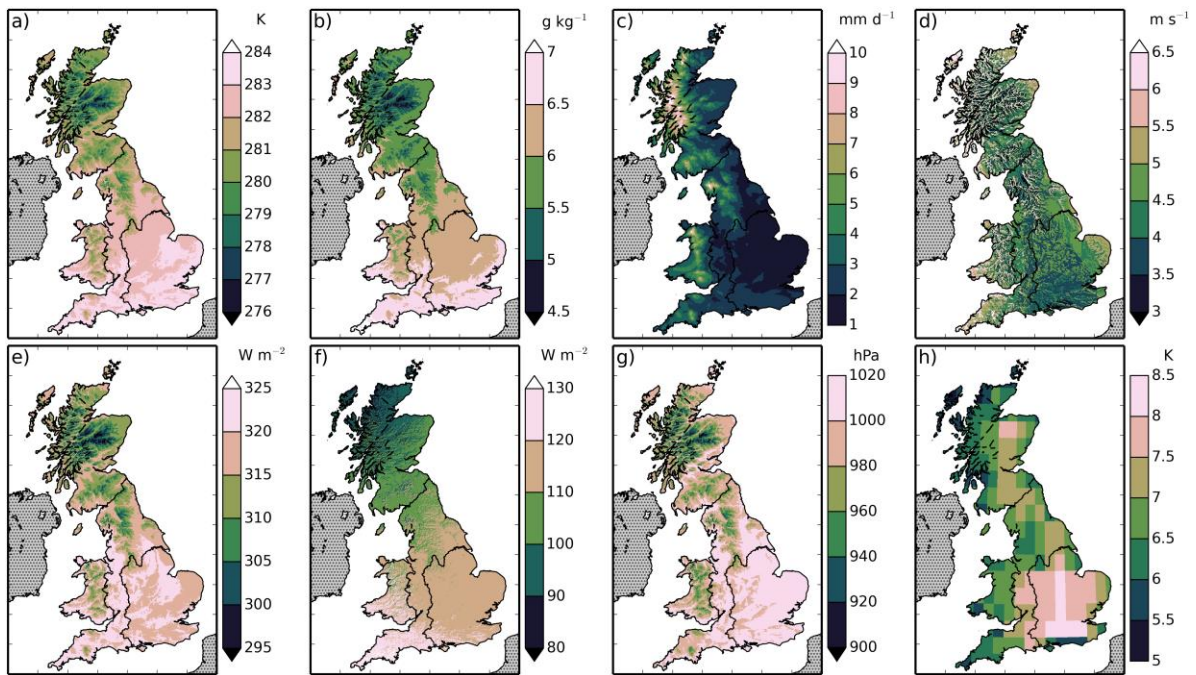
Site (ID)	Latitude	Longitude	Years	Land cover	Citation
Alice Holt (UK-Ham)	51.15	-0.86	2004-2012	Deciduous broadleaf woodland	(Wilkinson et al., 2012; Heinemeyer et al., 2012)
Griffin Forest (UK-Gri)	56.61	-3.80	1997-2001, 2004-2008	Evergreen needleleaf woodland	(Clement, 2003)
Auchencorth Moss (UK-AMo)	55.79	-3.24	2002-2006	Grass and crop	(Billett et al., 2004)
Easter Bush (UK-EBu)	55.87	-3.21	2004-2008	Grass	(Gilmanov et al., 2007; Soussana et al., 2007)

1393

1394 Table A2. Correlation statistics for meteorological variables with data from four sites.

a) Air temperature			
Site	$r^2$	Mean bias	RMSE
Alice Holt	0.95	0.10 K	1.17 K
Griffin Forest	0.94	0.21 K	1.17 K
Auchencorth Moss	0.98	-0.02 K	0.78 K
Easter Bush	0.97	-0.46 K	0.96 K
b) Downward SW radiation			
Site	$r^2$	Mean bias	RMSE
Alice Holt	0.94	-3.01 W m <sup>-2</sup>	22.92 W m <sup>-2</sup>
Griffin Forest	0.85	-4.90 W m <sup>-2</sup>	31.29 W m <sup>-2</sup>
Auchencorth Moss	0.91	14.27 W m <sup>-2</sup>	27.96 W m <sup>-2</sup>
Easter Bush	0.88	5.73 W m <sup>-2</sup>	27.15 W m <sup>-2</sup>
c) Mixing ratio			
Site	$r^2$	Mean bias	RMSE
Alice Holt	0.90	-0.02 mmol mol <sup>-1</sup>	1.09 mmol mol <sup>-1</sup>
Griffin Forest	0.76	0.08 mmol mol <sup>-1</sup>	1.56 mmol mol <sup>-1</sup>
d) Wind speed			
Site	$r^2$	mean bias	RMSE
Alice Holt	0.88	1.24 m s <sup>-1</sup>	1.45 m s <sup>-1</sup>
Griffin Forest	0.59	1.36 m s <sup>-1</sup>	1.81 m s <sup>-1</sup>
Auchencorth Moss	0.63	-0.38 m s <sup>-1</sup>	1.37 m s <sup>-1</sup>
Easter Bush	0.82	0.44 m s <sup>-1</sup>	1.03 m s <sup>-1</sup>
e) Surface air pressure			
Site	$r^2$	Mean bias	RMSE
Griffin Forest	0.05	-0.42 hPa	1.38 hPa
Auchencorth Moss	0.01	-1.06 hPa	1.57 hPa
Easter Bush	0.03	0.01 hPa	1.33 hPa

1395



1396

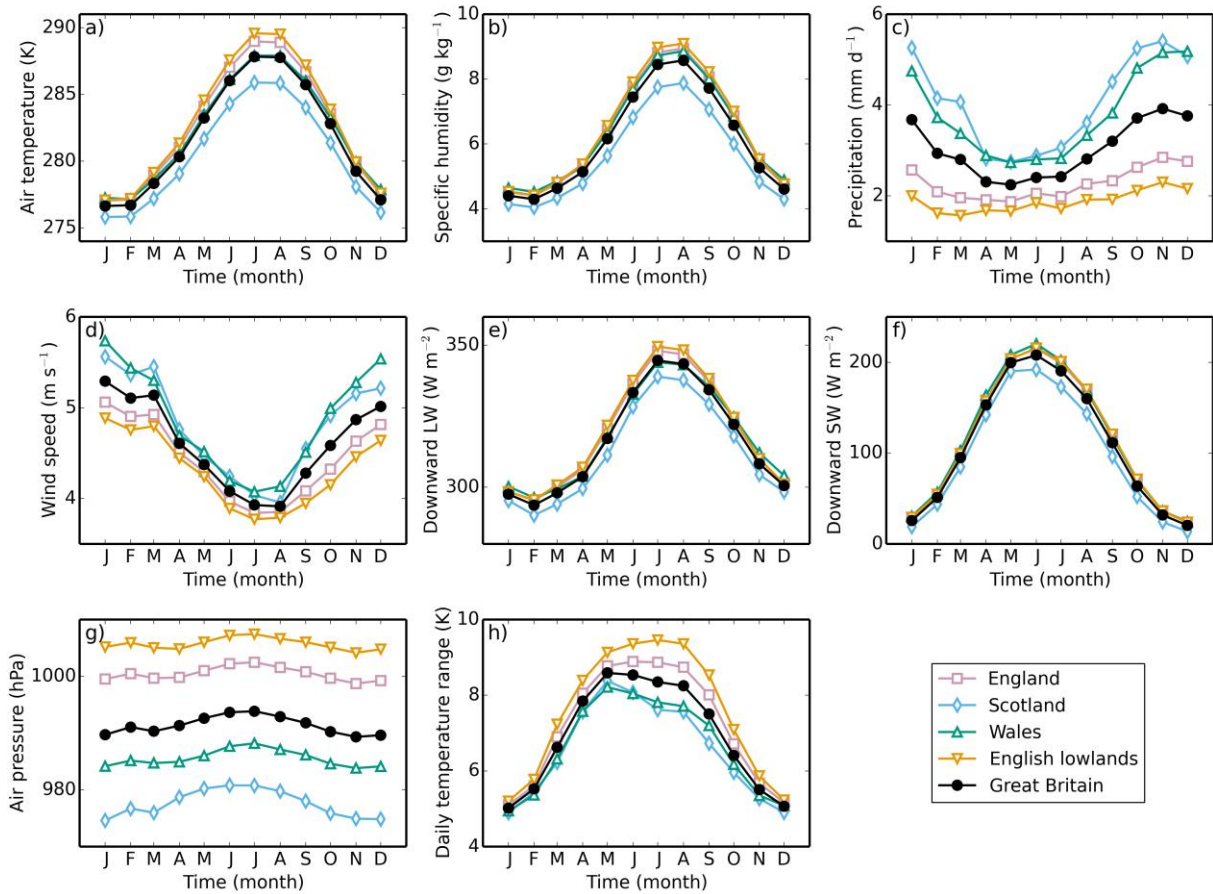
1397 Figure 1. Means of the meteorological variables over the years 1961-2012. The variables are  
 1398 a) 1.2 m air temperature, b) 1.2 m specific humidity, c) precipitation, d) 10 m wind speed, e)  
 1399 downward LW radiation, f) downward SW radiation, g) surface air pressure, h) daily air  
 1400 temperature range.



1401

1402 Figure 2. The regions used to calculate the area means. The English lowlands are a sub-region

1403 of England. England, Scotland and Wales together form the fifth region, Great Britain.

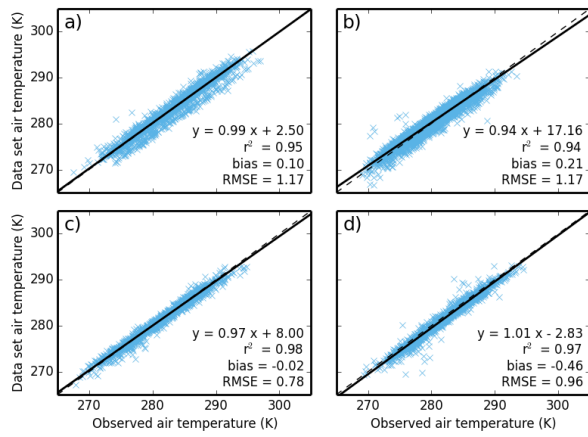


1404

1405 Figure 3. Mean monthly climatology of meteorological variables, a) 1.2 m air temperature, b)  
 1406 1.2 m specific humidity, c) precipitation, d) 10 m wind speed, e) downward LW radiation, f)  
 1407 downward SW radiation, g) surface air pressure, h) daily air temperature range, for five  
 1408 different regions of Great Britain, calculated over the years 1961-2012.

1409



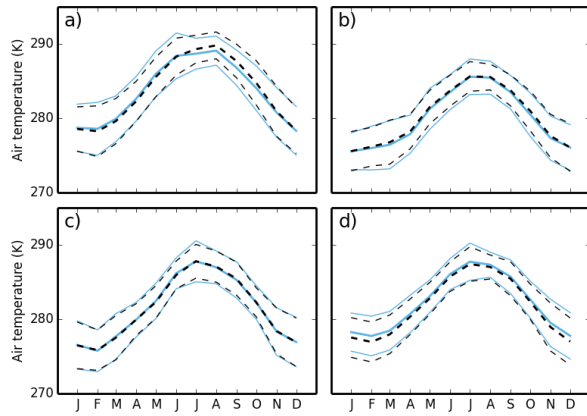


1410

1411 Figure 4. Plot of data set air temperature against daily mean observed air temperature at four  
 1412 sites. The dashed line shows the one to one line, while the solid line shows the linear regression,  
 1413 the equation of which is shown in the lower right of each plot, along with the  $r^2$  value, the mean  
 1414 bias and the RMSE. The sites are a) Alice Holt; b) Griffin Forest; c) Auchencorth Moss; d)  
 1415 Easter Bush.

1416

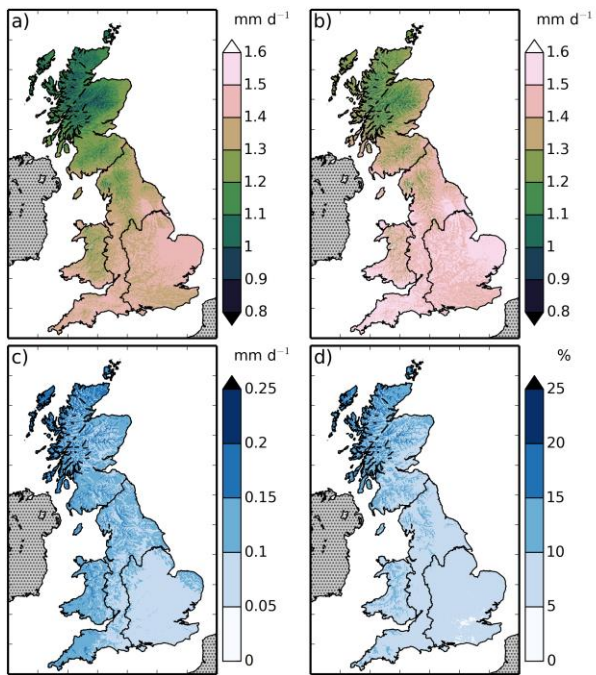
1417



1418

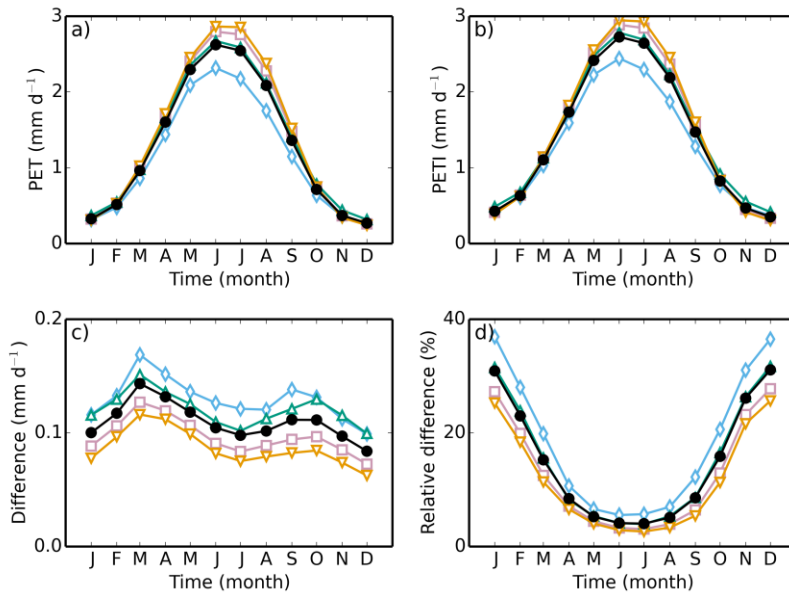
1419 Figure 5. Mean monthly climatology of the dataset (black, dashed lines) and observed (blue,  
1420 solid lines) air temperatures, calculated for the period of observations. The thicker lines show  
1421 the means, while the thinner lines show the standard errors on each measurement. Sites as in  
1422 Fig. 4.

1423



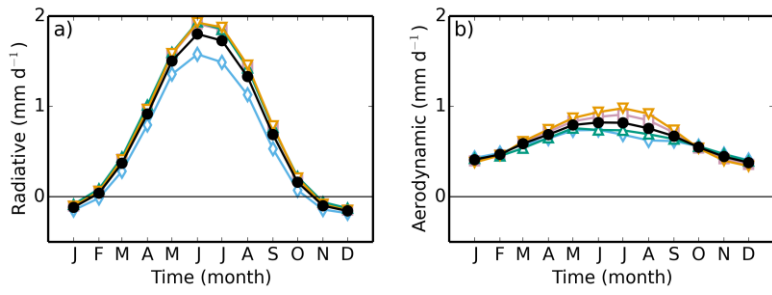
1424

1425 Figure 6. Mean a) PET, b) PETI, c) absolute difference between PETI and PET and d) relative  
 1426 difference calculated over the years 1961-2012.



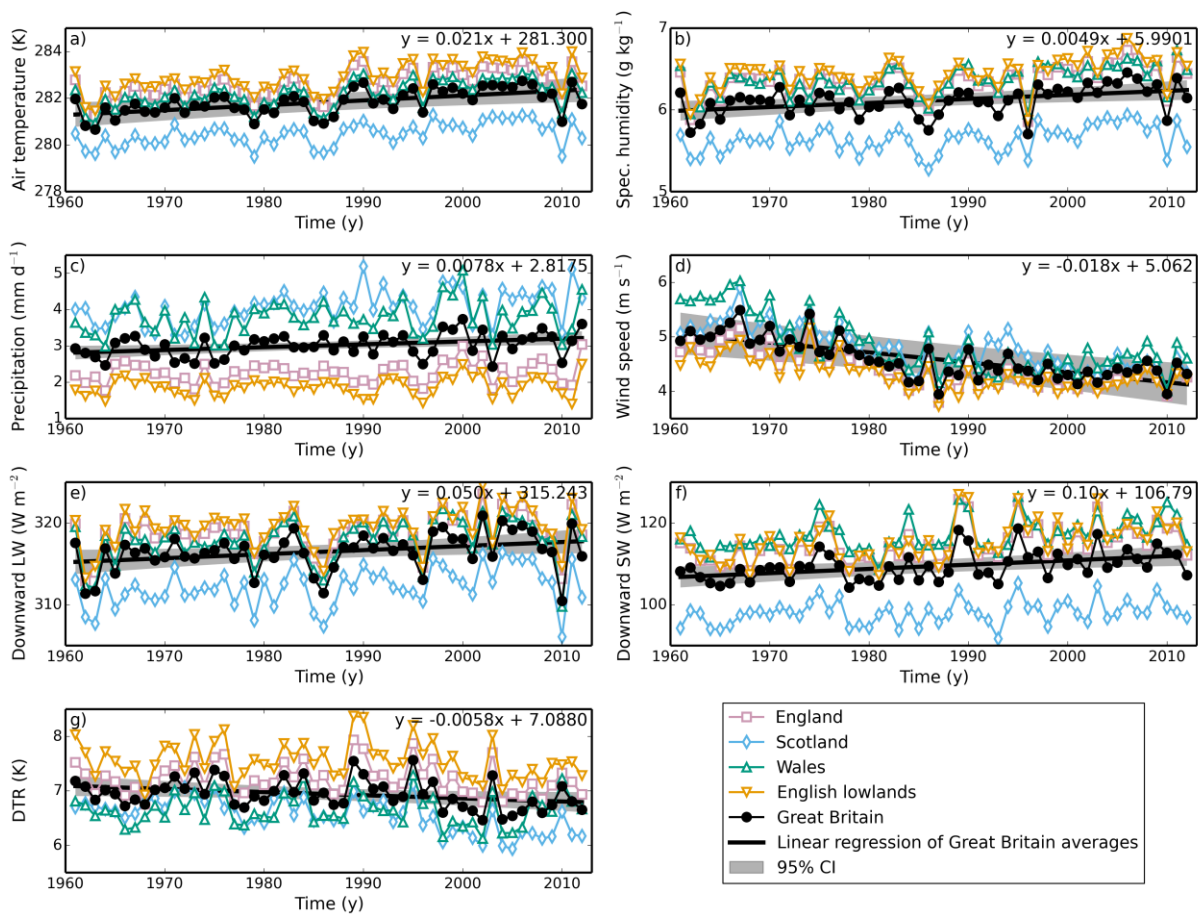
1427

1428 Figure 7. Mean monthly climatology of a) PET, b) PETI, c) absolute difference between PETI  
 1429 and PET, d) relative difference, for five different regions of Great Britain, calculated over the  
 1430 years 1961-2012. Symbols as in Fig. 3.



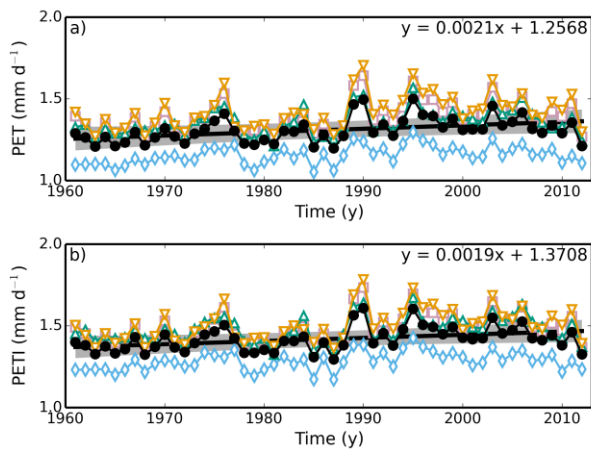
1431

1432 Figure 8. Mean-monthly climatology of the a) radiative and b) aerodynamic components of the  
 1433 PET for five different regions of Great Britain, calculated over the years 1961-2012. Symbols  
 1434 as in Fig. 3.



1435

1436 Figure 9. Annual means of the meteorological variables, a) 1.2 m air temperature, b) 1.2 m  
 1437 specific humidity, c) precipitation, d) 10 m wind speed, e) downward LW radiation, f)  
 1438 downward SW radiation, g) daily air temperature range, over five regions of Great Britain. The  
 1439 solid black lines show the linear regression fit to the Great Britain annual means, while the grey  
 1440 strip shows the 95% CI of the same fit, assuming a non-zero lag-1 correlation coefficient. The  
 1441 equation of this fit is shown in the top right-hand corner of each plot.

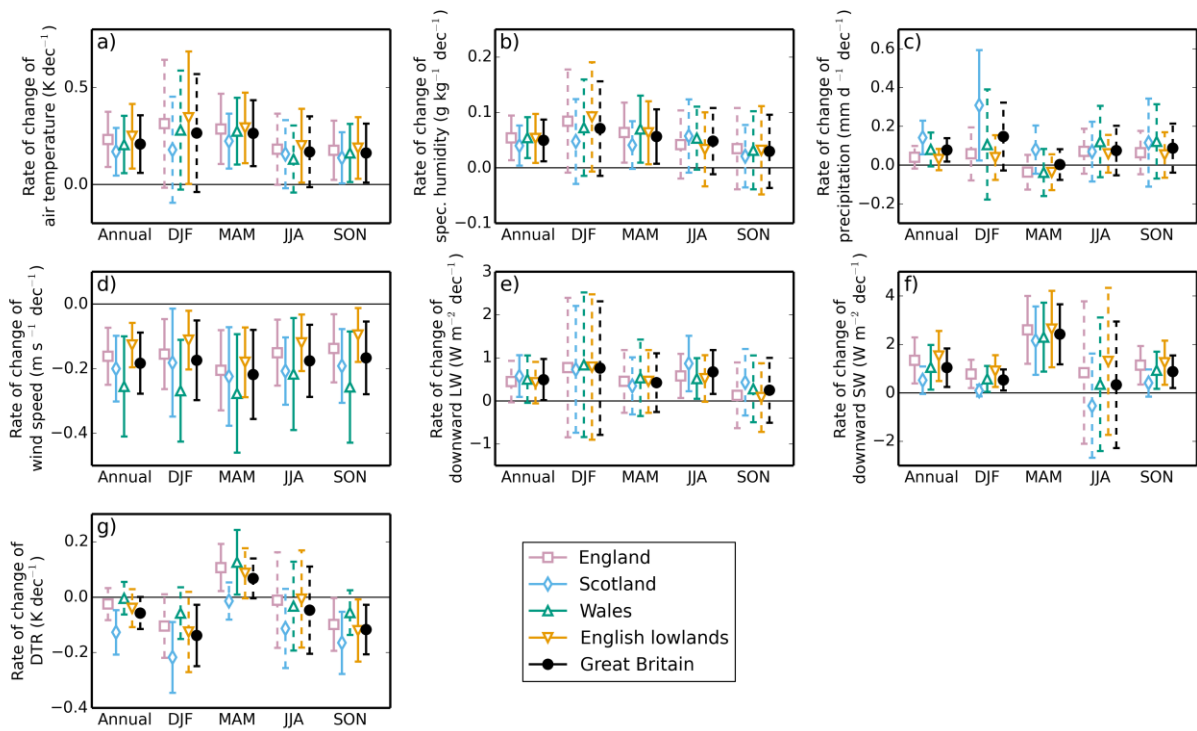


1442

1443 Figure 10. Annual means of a) PET and b) PETI for five regions of Great Britain. Symbols as

1444 in Fig. 9.

1445

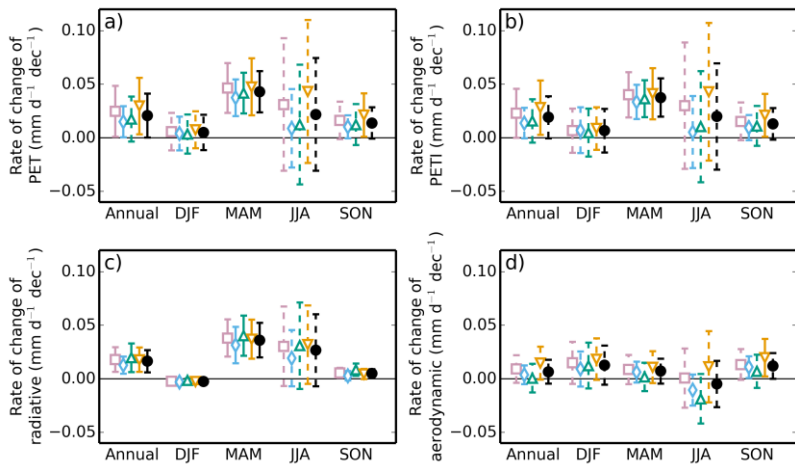


1446

1447 Figure 11. Rate of change of annual and seasonal means of meteorological variables, a) 1.2 m  
 1448 air temperature, b) 1.2 m specific humidity, c) precipitation, d) 10 m wind speed, e) downward  
 1449 LW radiation, f) downward SW radiation, g) daily air temperature range, for five regions of  
 1450 Great Britain for the years 1961-2012. Error bars are the 95% CI calculated assuming a non-  
 1451 zero lag-1 correlation coefficient. Solid error bars indicate slopes that are statistically significant  
 1452 at the 5% level, dashed error bars indicate slopes that are not significant at the 5% level.

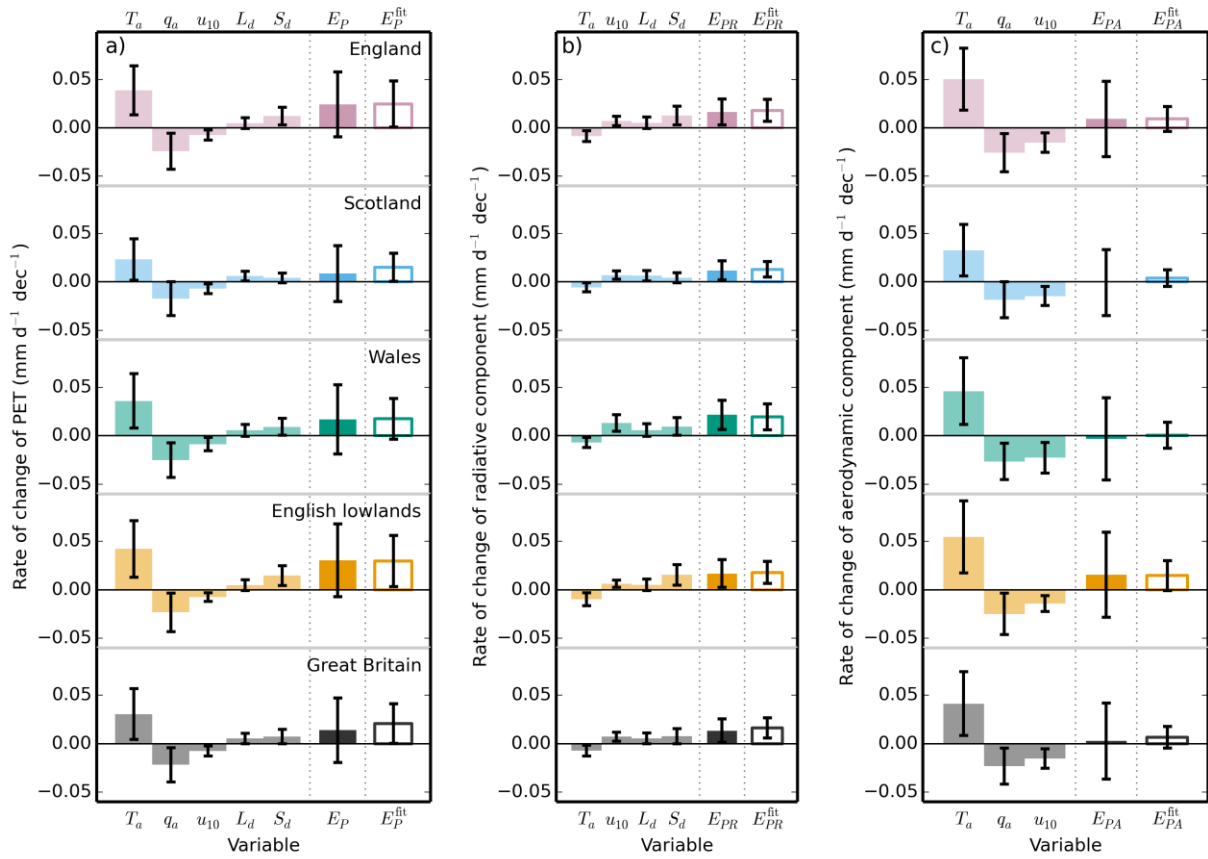
1453





1454

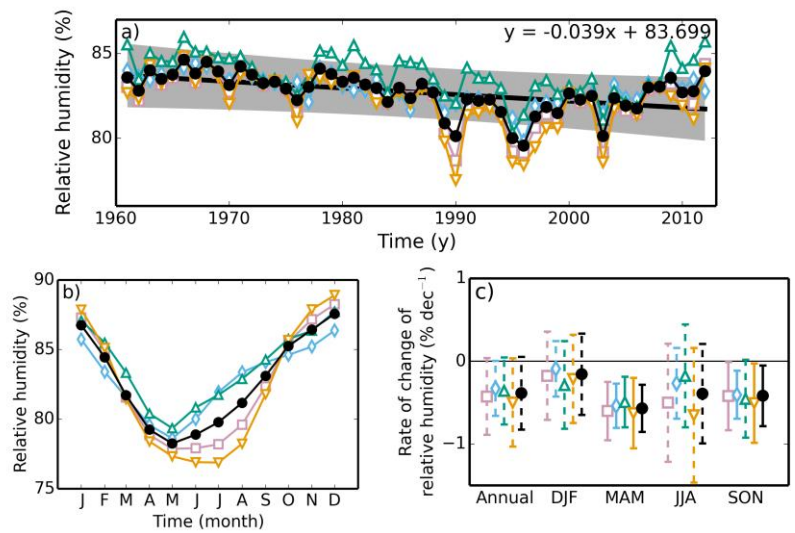
1455 Figure 12. Rate of change of annual and seasonal means of a) PET, b) PETI, c) the radiative  
 1456 component of PET and d) the aerodynamic component of PET for five regions of Great Britain  
 1457 for the years 1961-2012. Symbols as in Fig. 11.



1458

1459 Figure 13. The contribution of the rate of change of each meteorological variable to the rate of  
 1460 change of a) PET, b) the radiative component and c) the aerodynamic component. The first five  
 1461 (four; three) bars are the contribution to the rate of change of annual mean PET from the rate  
 1462 of change of each of the variables, calculated per pixel, than averaged over each region. Each  
 1463 bar has an error bar showing the 95% CI on each value. Since the pixels are highly spatially  
 1464 correlated, we use the more conservative CI calculated by applying this analysis to the regional  
 1465 means. The next bar is the sum of the other bars and shows the attributed rate of change of  
 1466 annual mean PET. The final bar shows the slope and its associated CI obtained from the linear  
 1467 regression of the mean annual PET for each region.

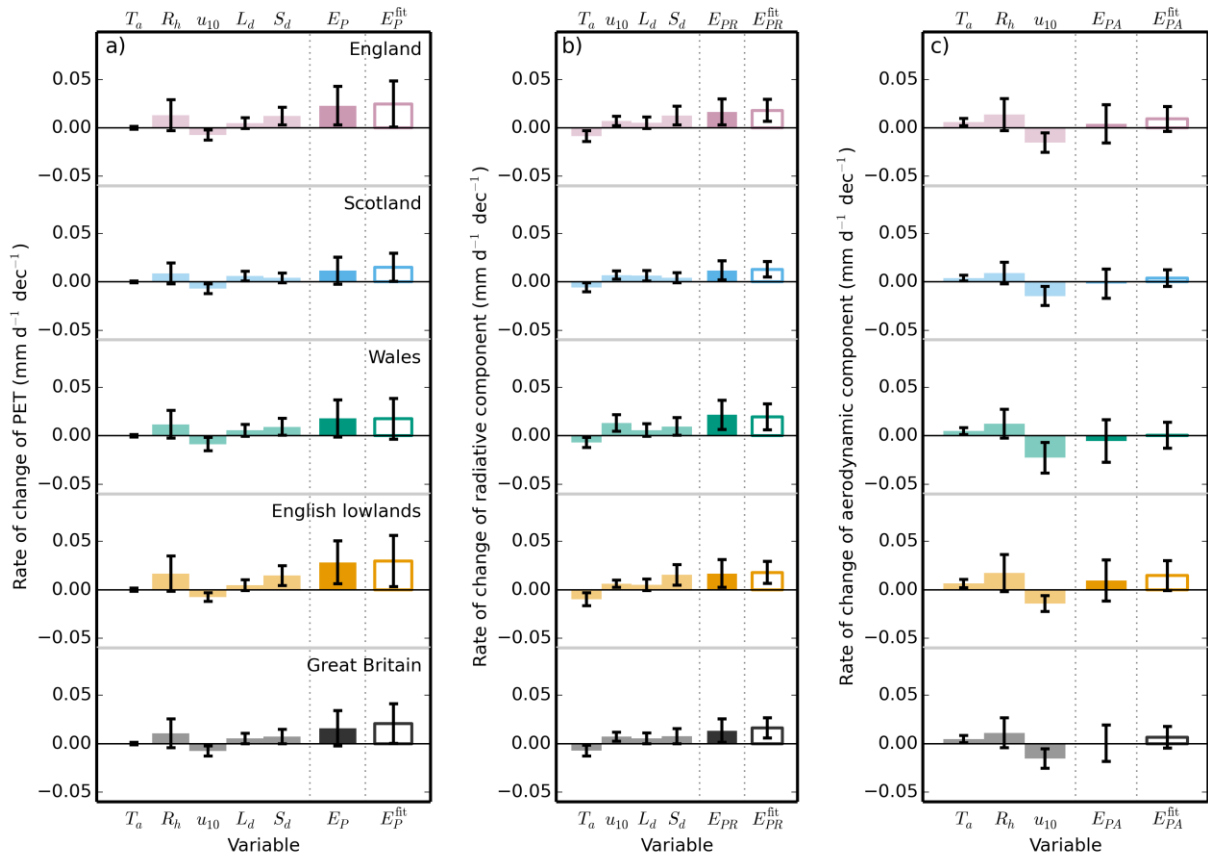
1468



1469

1470 Figure 14. Regional annual means (a), regional mean-monthly climatology (b) and regional  
 1471 rates of change of relative humidity for the years 1961-2012.

1472

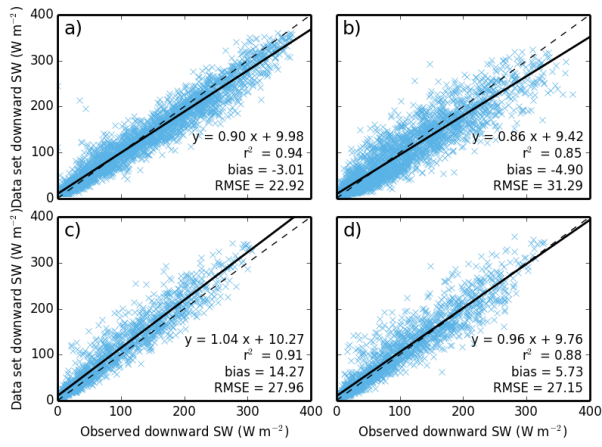


1473

1474 Figure 15. The contribution of the rate of change of each meteorological variable to the rate of  
 1475 change of a) PET, b) the radiative component and c) the aerodynamic component, with relative  
 1476 humidity instead of specific humidity. The first five (four; three) bars are the contribution to  
 1477 the rate of change of annual mean PET from the rate of change of each of the variables,  
 1478 calculated per pixel, than averaged over each region. Each bar has an error bar showing the  
 1479 95% CI on each value. Since the pixels are highly spatially correlated, we use the more  
 1480 conservative CI calculated by applying this analysis to the regional means. The next bar is the  
 1481 sum of the other bars and shows the attributed rate of change of annual mean PET. The final  
 1482 bar shows the slope and its associated CI obtained from the linear regression of the mean annual  
 1483 PET for each region.

1484

1485



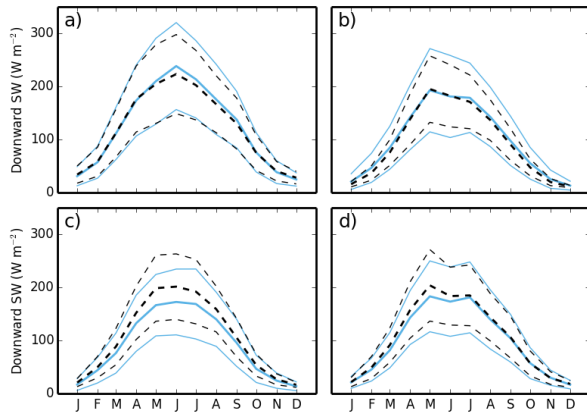
1486

1487 Figure A1. Plot of data set downward SW radiation against daily mean observed downward

1488 SW radiation at four flux sites. Symbols and sites as in Fig. 4.

1489

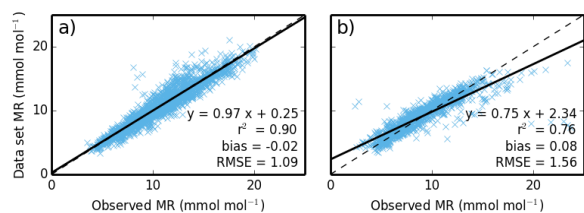
1490



1491

1492 Figure A2. Mean monthly climatology of the dataset (black, dashed lines) and observed (blue,  
1493 solid lines) downward SW radiation, calculated for the period of observations. Symbols as in  
1494 Fig. 5, sites as in Fig. 4.

1495

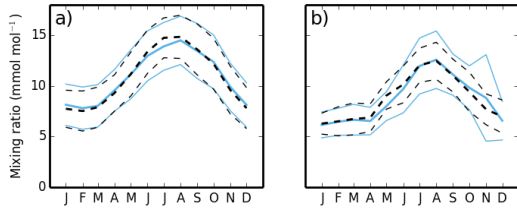


1496

1497 Figure A3. Plot of mixing ratio calculated using dataset meteorology against daily mean  
1498 observed mixing ratio at four sites. Symbols as in Fig. 4. The sites are a) Alice Holt and b)  
1499 Griffin Forest.

1500

1501

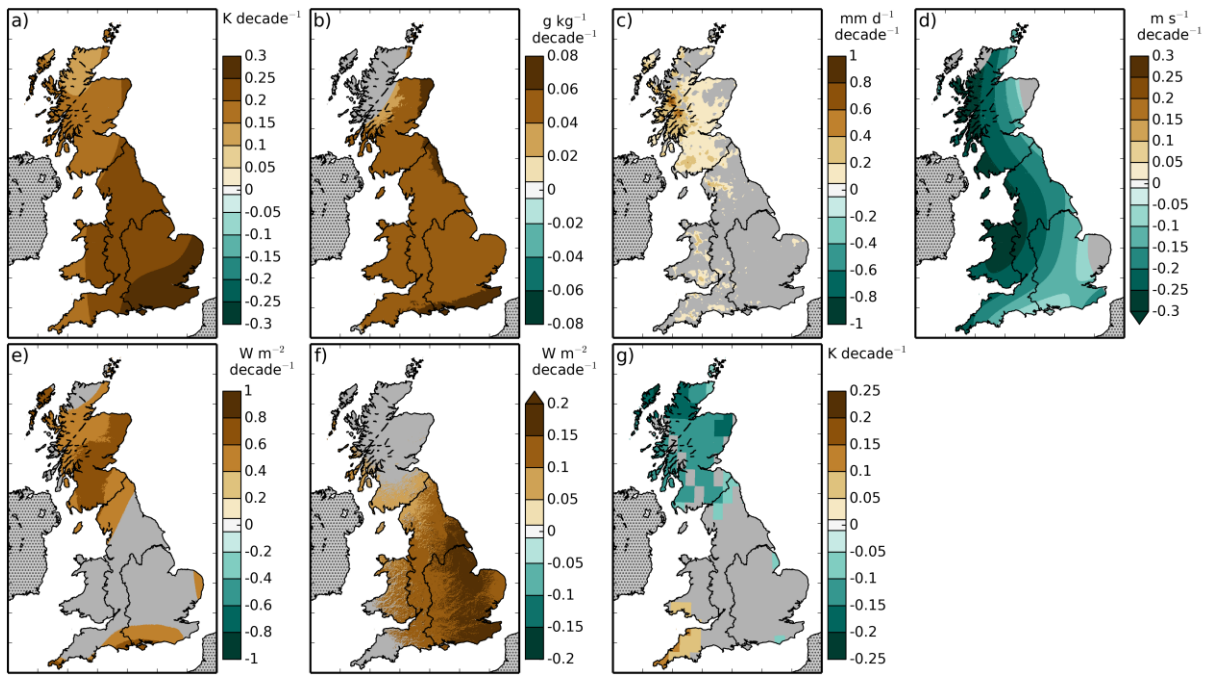


1502

1503 Figure A4. Mean monthly climatology of the dataset (black, dashed lines) and observed (blue,  
1504 solid lines) mixing ratio, calculated for the period of observations. Symbols as in Fig. 5. Sites  
1505 as in Fig. A3.

1506

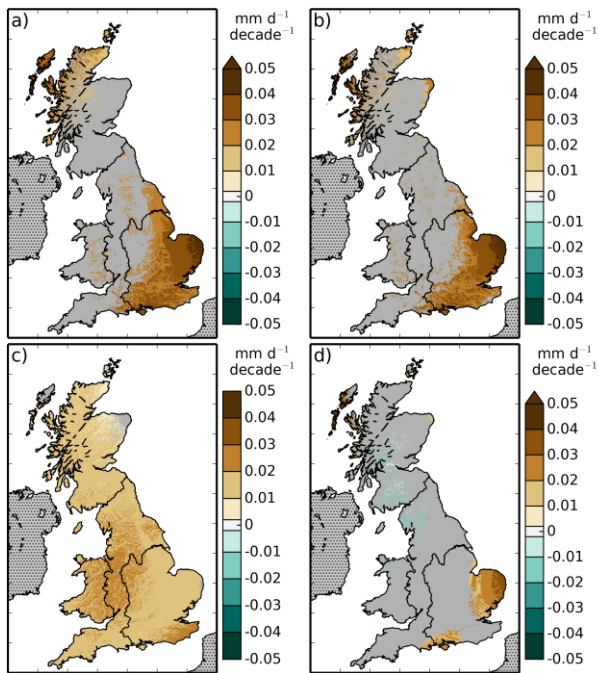




1507

1508 Figure B1. Rate of change of the annual means of the meteorological variables, a) 1.2 m air  
 1509 temperature, b) 1.2 m specific humidity, c) precipitation, d) 10 m wind speed, e) downward LW  
 1510 radiation, f) downward SW radiation, g) daily air temperature range over the period 1961-2012.  
 1511 Areas for which the trend was not significant are shown in grey.

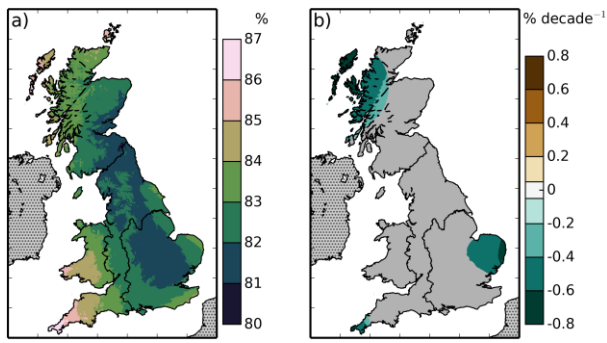
1512



1513

1514 Figure B2. Rate of change the annual means of a) PET, b) PETI, c) the radiative component of  
 1515 PET, d) the aerodynamic component of PET over the period 1961-2012. Areas for which the  
 1516 trend was not significant are shown in grey.

1517



1518

1519 Figure B3. Maps of a) mean and b) rate of change of annual mean of the relative humidity over  
1520 the years 1961-2012. Areas for which the trend was not significant are shown in grey.

1521